Chapter 10
Spacecraft Antenna Research and Development Activities Aimed at Future Missions

John Huang

Space missions of the Jet Propulsion Laboratory (JPL) of the National Aeronautics and Space Administration (NASA) can be categorized into two major areas: deep-space exploration and Earth remote sensing. As scientists have learned from the previous missions, higher capabilities and more stringent system requirements are being placed on future missions, such as longer distance communications, higher data rate, and finer radar imaging resolution. Almost all these stringent requirements call for higher-gain and larger-aperture spacecraft antennas. At the same time, however, lower mass and smaller stowage volume for the spacecraft antenna are demanded in order to reduce payload weight and reduce required shroud space, and thus minimize overall launch cost. To meet these goals, several space-deployable antenna concepts [1] have been investigated over the past several decades. To name a few, there were the Harris Corporation's hoop-column umbrella type, Lockheed's wrapped-rib version, TRW's sunflower antenna, and the more recent Astro mesh. All these deployable antennas are of the parabolic reflector type with metalized mesh reflecting surfaces. Because they have been parabolic with a relatively small focal length, they lack wide-angle beam scanning ability—only a few beamwidths can be scanned. The mesh surface also limits the upper frequency of operation to Ku-band or lower. In addition, some of these concepts suffer from higher risk because of too many mechanical components. One good example of mechanical component failure is the Galileo spacecraft,

which used the Harris radial rib mesh reflector that failed to deploy in space. To remedy these drawbacks, several new antenna concepts are being investigated at JPL for possible future-mission applications. These antenna concepts, separately discussed below, are the inflatable array antenna, foldable thin-membrane array, and reflectarray. The mechanical characteristics of inflatable antennas are discussed in Chapter 8. In addition, the wide swath ocean altimeter (WSOA) a reflectarray developed for, but not used on, the Ocean Surface Topography Mission (OSTM) is discussed in Section 7.6.

10.1 Inflatable Array Antenna

A deployable antenna using inflatable parabolic reflector concept was introduced [2] in the mid 1980s for achieving large aperture with low mass and small stowage volume. This concept was later demonstrated in a space shuttle (Endeavour STS-77 mission) experiment in 1996 [3] called the In-space Antenna Experiment (IAE), which used a 14-m diameter thin-membrane reflector (see also Section 8.1.6). The antenna, as shown in Fig. 10-1, had an annular inflatable tube to support a thin-membrane parabolic surface and three inflatable tubular struts to support a possible feed. This large-aperture antenna was successfully deployed in space, but, by a large margin, failed to meet the required surface tolerance. Thus, the full implementation of this concept is still hampered by the inability to achieve and maintain the required surface accuracy. In particular, it is believed that it would be difficult to maintain the

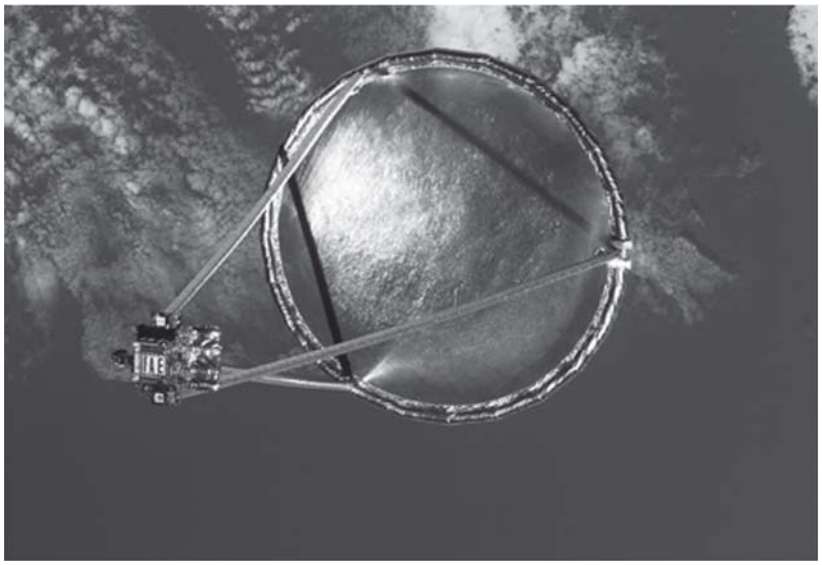

Fig. 10-1. Actual space-flight photo of the 14-m inflatable parabolic reflector (a Space Shuttle experiment in 1996).

desired surface accuracy of a large thin-membrane parabolic surface over the duration of a long space flight. To mitigate the difficulty associated with curved surfaces, a new class of deployable planar array technology is being developed [4,5]. It is believed that it would be significantly more reliable to maintain the required surface tolerance of a flat "natural" surface, such as a planar array, than a specifically curved "non-natural" surface, such as a parabolic reflector. In addition, a planar array offers the possibility of wide-angle beam scanning, which cannot be easily achieved by a parabolic reflector.

At JPL, two types of inflatable planar array antennas have recently been developed [6]. One is the inflatable synthetic aperture radar (SAR) multilayer microstrip array for Earth remote sensing at the L-band frequency. The other is the inflatable microstrip reflectarray for deep-space telecom application at the Ka-band frequency. Most of the radio frequency (RF) capabilities and a portion of the space-environment mechanical capabilities have already been demonstrated for these two antenna types under JPL efforts. The RF designs and the aperture membrane surfaces of these antennas were developed at JPL, while the inflatable structure developments and antenna integrations were mostly accomplished by ILC Dover, Inc. and L'Garde Corp. under JPL contracts. All these antennas were constructed and developed in a similar fashion with each basically constructed from an inflatable tubular frame that supports and tensions a multilayer thin-membrane RF radiating surface. They are deployed by a "rolling" mechanism, rather than by the "folding" mechanism. Multi-folding of the thin membrane radiating surface has not been used here to avoid the forming of large creases on the printed patch elements and transmission lines. Any large crease may significantly degrade the impedance matching of the microstrip circuit and hence the overall RF performance. As is shown later, these antenna developments have demonstrated that inflatable thin-membrane arrays are feasible across the microwave and millimeter-wave spectra. Further developments of these antennas are deemed necessary, in particular, in the area of qualifying the inflatable structures for space environment usage. The detailed description and performance of these two types of inflatable array antennas are separately presented in the following subsections.

10.1.1 Inflatable L-Band SAR Arrays

10.1.1.1 Antenna Description. The inflatable L-band SAR array, having an aperture size of 3.3 m × 1.0 m, is a technology demonstration model with 1/3 the size of the future full size (10 m × 3 m) array. Two such inflatable arrays were recently developed: one by ILC Dover, Inc. and the other by L'Garde Corp. For both antennas, the concepts and electrical designs were accomplished at JPL, while the inflatable structures were developed by the two companies. The ILC Dover unit is shown in Fig. 10-2, and the L'Garde unit is shown in

Fig. 10-3. Both units are very similar, and each basically is a rectangular frame of inflatable tubes that supports and tensions a three-layer thin-membrane radiating surface with microstrip patches and transmission lines. The inflatable tube of the ILC Dover unit has a diameter of 13 cm and is made of 0.25-mm thick urethane coated Kevlar material. The L'Garde's inflatable tube has a diameter of 9 cm and is made of 0.08-mm-thick rigidizable stretched aluminum material. The inflatable tubes need to be rigidized once they are deployed in space so that they could avoid the need of constant air pressure and the concern of air leakage due to space debris damage. This technology of tube rigidization is further discussed in Section 10.1.3.2. The three membrane layers are separated 1.27 cm between the top radiator layer and the middle ground-plane layer and 0.635 cm between the middle layer and the bottom transmission-line layer. The bottom transmission lines excite the top radiating patches, not by rigid feed-through pins, but by a set of aperture coupling slots [7] so that no

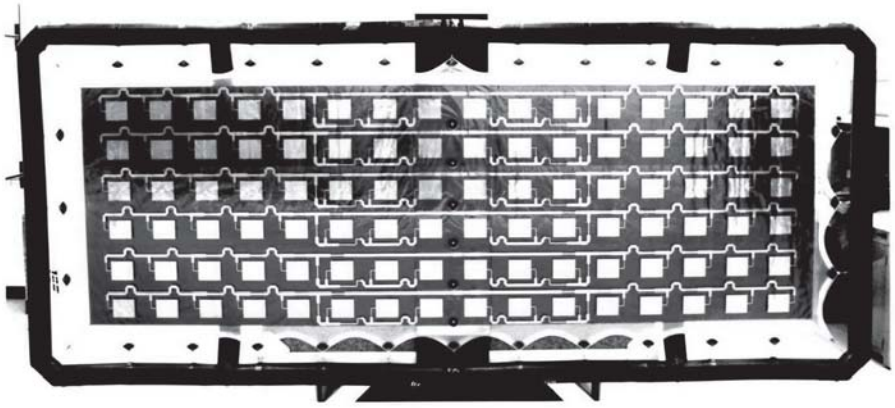

Fig. 10-2. Inflatable L-band SAR array (3.3 m × 1 m) developed by JPL and ILC Dover Inc.

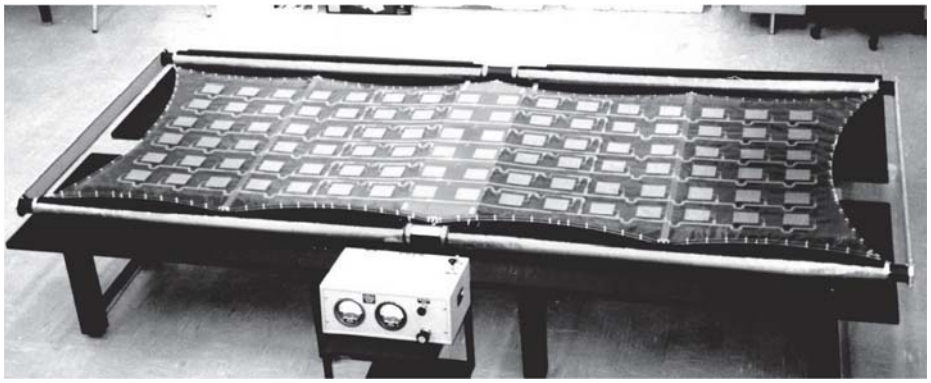

Fig. 10-3. Inflatable L-band SAR array (3.3 m × 1 m) developed by JPL and L'Garde Corp.

soldering is required here. The connection between the edges of these membranes and the inflated tubular frame is made by a series of catenary attachment points and tensioning cords. The required spacings between the three membranes are maintained by the tensioning of the catenary cords, the honeycomb spacing panels and bars, and small spacer blocks at each of the catenary points. The membrane material used is a thin film of 5-μm thick copper cladding on a 0.13-mm thick Kapton dielectric material. It should be noted that all metal claddings (radiating elements, transmission lines, and ground plane) should have a minimum thickness of at least twice the skin depth at the operating frequency. Otherwise, radiation will leak through the thin metal and reduce the antenna efficiency.

10.1.1.2 Antenna Test Results. The L'Garde unit achieved a total antenna mass of 11 kg with an average mass density of 3.3 kg/m^2. The ILC Dover unit has a slightly higher mass. The surface flatness of the L'Garde unit was measured to be ±0.28 mm, which is better than the requirement of ±0.8 mm. The ILC Dover's surface flatness was measured to be ±0.7 mm. Both antenna units achieved bandwidths slightly wider than the required 80 MHz, and achieved port isolation between the two orthogonal polarizations of greater than 40 dB within the required bandwidth. The radiation patterns of the ILC Dover unit measured in two principal planes at 1.25 gigahertz (GHz) are given in Fig. 10-4. Sidelobe levels of –14 dB in the azimuth plane and –12 dB in the elevation plane are reasonable for this uniformly distributed array. The cross-polarization level of less than –20 dB within the main beam region is also considered acceptable for this radar application. Patterns measured at frequencies from 1.21 to 1.29 GHz are very similar to those shown in Fig. 10-4 without significant degradation. The measured peak gain of ILC Dover's unit is 25.2 dB at 1.25 GHz, which corresponds to an aperture efficiency of 52 percent. L'Garde's unit has a peak gain of 26.7 dB and an aperture efficiency of 74 percent. The better efficiency of L'Garde's unit is the result of better surface tolerance and more precise membrane spacing. Nevertheless, both units are considered quite good as they are the first demonstration models ever developed. Both these inflatable array antennas had masses less than half of those with rigid structures, while achieving similar radiation efficiencies. Although another type of deployable antenna with mesh structure achieved similar, or even in some cases smaller masses, these mesh antennas can only be used as reflectors but not as arrays.

10.1.2 Ka-Band 3-m Reflectarray

10.1.2.1 Antenna Description. The details of the reflectarray antenna technology are discussed further in Section 10.4. The reflectarray is used here because of its unique feature of having a flat reflecting aperture. A photograph

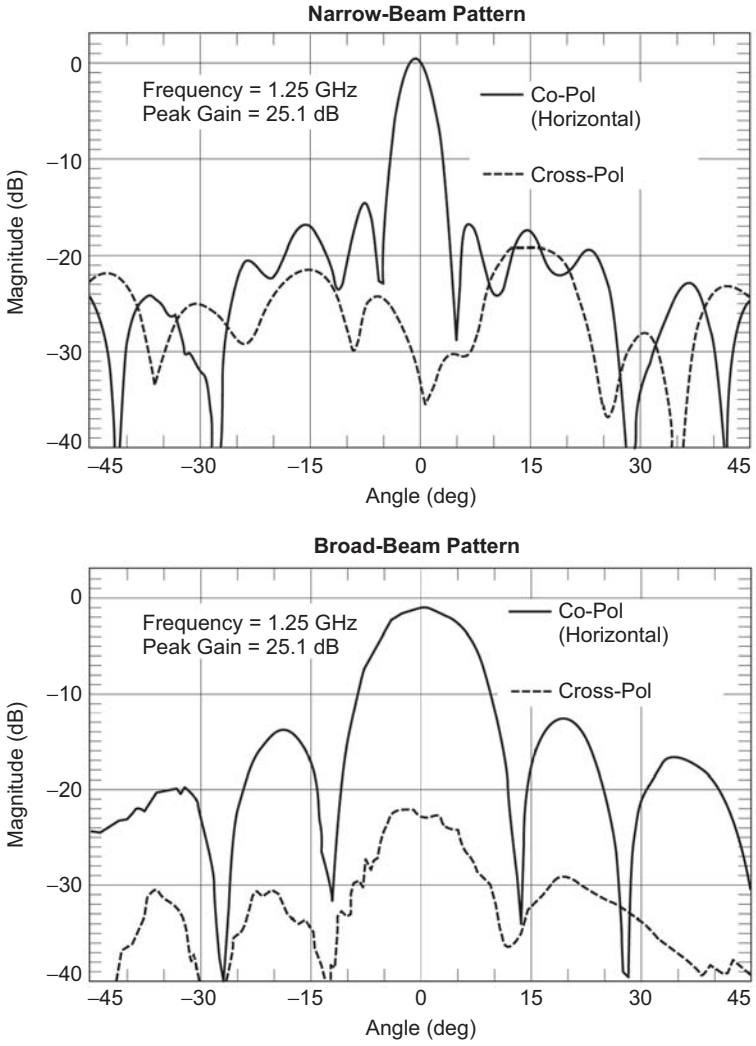

Fig. 10-4. Measured two principal-plane patterns of the ILC Dover inflatable array for (a) narrow-beam pattern, (b) broad-beam pattern.

of the inflatable Ka-band reflectarray antenna with a 3-m diameter aperture is shown in Fig. 10-5. This antenna was co-developed by JPL and ILC Dover, Inc. It consists of a horseshoe shaped inflatable tube that supports and tensions a 3-m aperture membrane. The tube, 25 cm in diameter, is made of urethane-coated Kevlar and is inflated to 3.0 pound-per-square-inch (psi) (21 kPa) pressure, which translates to about 90 psi (620 kPa) of tension force to the aperture membrane. The inflatable tube is connected to the aperture membrane at 16 catenary points with spring-loaded tension cords. Each connecting point has displacement adjustment capability in the x, y, z directions so that the

Fig. 10-5. Inflatable Ka-band 3-m reflectarray antenna. The white-colored structure in front of the aperture is a membrane-flatness measurement device.

circumference of the circular aperture membrane can be made into a single plane orthogonal to the feedhorn axis. The single-layer aperture membrane is a 5-mil (0.13-mm) thick Uplex dielectric material (a brand of polyimide) with both sides clad with 5-μm thick copper. The copper on one side is etched to form approximately 200,000 microstrip patch elements, while the copper on the other side is un-etched and serves as the ground plane for the patch elements. Portion of the microstrip elements are shown in Fig. 10-6. The elements use a variable rotation technique [8] to provide the needed electrical phases. The inflatable tripod tubes, asymmetrically located on the top portion of the horseshoe structure, are used to support a Ka-band corrugated feedhorn. The horseshoe-shaped main tube structure and the asymmetrically connected tripod tubes are uniquely designed in geometry to avoid membrane damage and flatness deviation when the deflated antenna structure is rolled up.

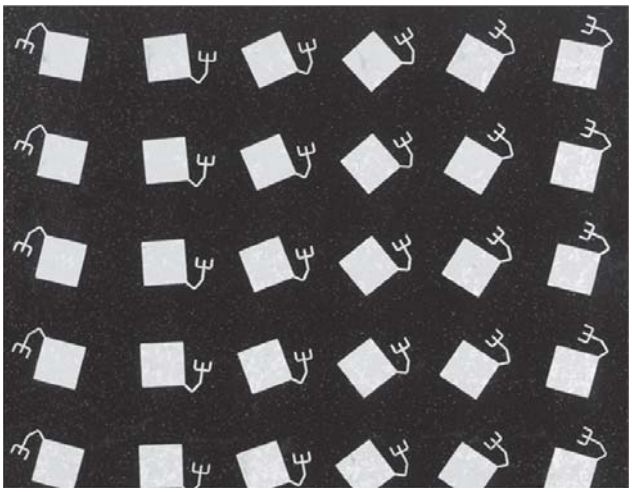

Fig. 10-6. Close-up view of the Ka-band reflectarray patch elements. A rotational technique is used to achieve the desired element electrical phase.

10.1.2.2 Antenna Test Results. The antenna's RF tests were performed at the in-door compact range of Composite Optics, Inc. (COI), where antennas as large as 10 m can be tested. Figure 10-7 shows a typical elevation pattern of the antenna with measurements of a 0.22-deg beamwidth. The sidelobe level is –30 dB or lower below the main beam peak, and the cross-polarization level is –40 dB or lower. All patch elements are circularly polarized and are identical in dimensions. Their angular rotations are different and are designed to provide correct phase delays to achieve a co-phasal aperture distribution. The antenna gain was measured versus frequency. The results show that the antenna is tuned to the desired frequency of 32.0 GHz with a –3-dB bandwidth of 550 MHz. A peak gain of 54.4 decibels referenced to a circularly polarized, theoretical isotropic radiator (dBic) was measured. This measured antenna gain indicates an aperture efficiency of 30 percent, which is lower than the expected 40 percent. This relatively lower efficiency was the result of large element resistive loss due to the poor loss-tangent material of Kapton used, non-optimal substrate thickness, large feed-struts blockage, and non-optimal feed illumination. The phase delay line that is attached to each patch element has a certain amount of impedance mismatch to the patch, and thus, sends a certain amount of RF power into undesirable cross-polarization energy, and this results in poor radiation efficiency. It is quite certain that future development can improve the efficiency to the expected 40 percent or higher. The measured surface flatness data of the antenna aperture shows a root mean square (RMS) value of 0.2 mm, while the required surface RMS value is 0.5 mm. This good surface flatness is also reflected by the well-formed far-field pattern with

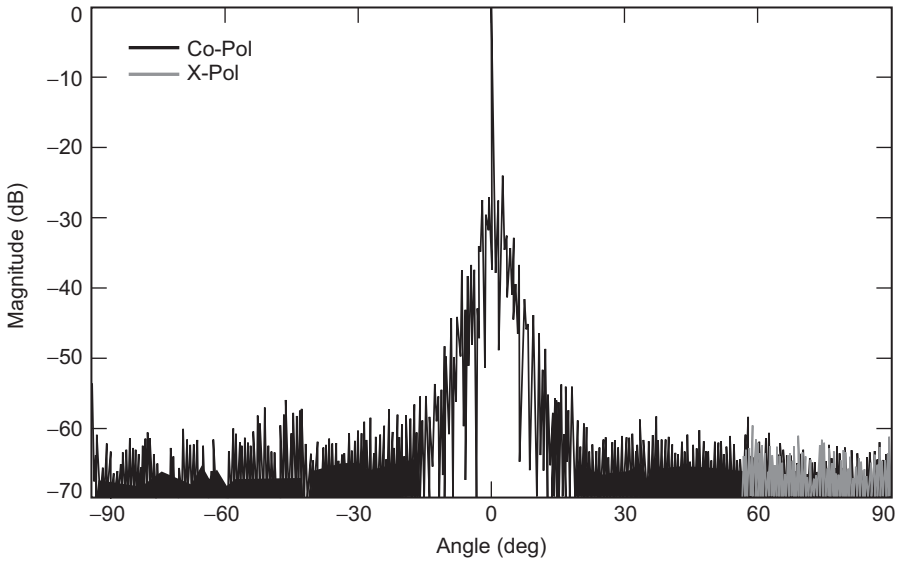

Fig. 10-7. Measured radiation pattern of the 3-m Ka-band inflatable reflectarray.

expected main beamwidth and low sidelobe level. A solid antenna can certainly achieve surface flatness better than 0.2 mm rms, but with significantly increased mass. Although the aperture efficiency of the inflatable reflectarray was not as expected, the achievement of excellent membrane flatness indicates that inflatable array antenna at Ka-band is now feasible.

10.1.2.3 Improved Ka-Band 3-m Reflectarray. The above Ka-band 3-m inflatable reflectarray was built primarily for laboratory demonstration of its RF performance only. Since then, a second model was developed to demonstrate its mechanical integrity. There are two major differences in the models. One is that the second model has its inflatable reflectarray surface deployed without the deployment of a tripod-supported feed. The offset feed is fixed on the spacecraft bus as illustrated in Fig. 10-8, where the inflatable surface, shown in Fig. 10-9, can be rolled up and down as a movie screen. The second major difference is that the inflatable tubes are made of rigidizable aluminum reinforced internally by using carpenter extendable-ruler tapes as shown in Fig. 10-10. This type of tube is named spring-tape reinforced (STR) boom. Once the booms are inflated in space, the aluminum membrane soon rigidizes (see Section 10.1.3.2), and the inflation gas is no longer needed. In addition, in the event that the tubes are penetrated by small space debris, they will remain rigid to provide proper support for the reflectarray membranes. The carpenter tapes are used as reinforcement to provide additional axial load capacity as well as some orthogonal load capacity to each tube.

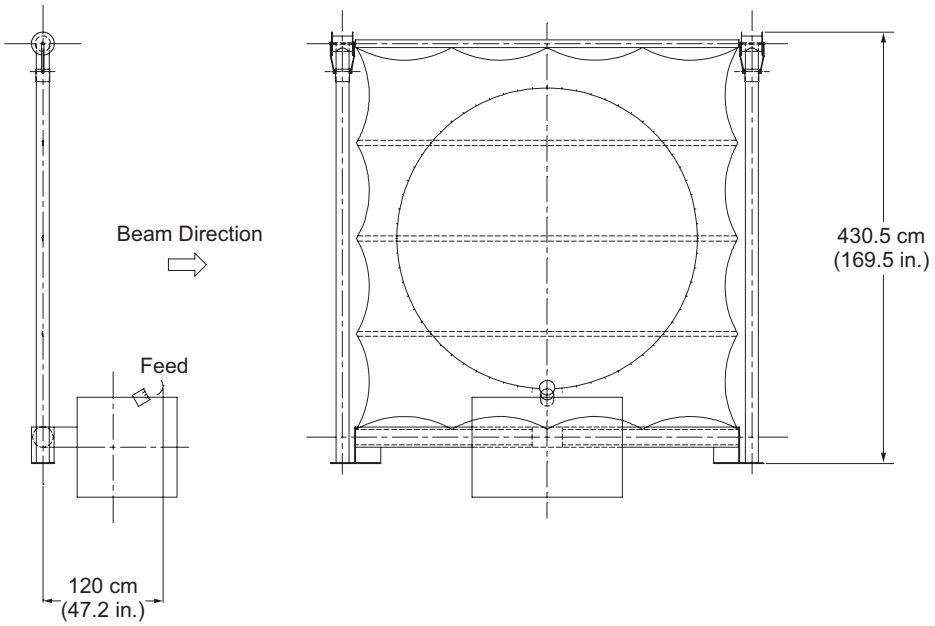

Fig. 10-8. Configuration of offset-fed inflatable reflectarray on spacecraft (rectangular box). Inflatable tubes allow the aperture to roll up.

10.1.2.4 Thermal Analysis of the Inflatable Reflectarray. The most critical structural components of the 3-m inflatable reflectarray antenna, illustrated in Fig. 10-8, are the two STR aluminum laminate inflatable/self-rigidizable booms [9]. Due to other mechanical reasons, these two booms cannot be thermally protected with thermal blankets and will undergo thermal distortions in space. This section presents results of a study of structural integrity of these booms under space thermal environments, as well as the effects of thermal distortion of the booms on surface deviation of the RF membrane [10].

The in-space structural integrity of these booms is first investigated. After in-space deployment of the antenna, the two STR booms are continuously loaded by axial forces that react to the tension in the RF membrane. The two booms will also bow due to the circumferentially uneven thermal expansions. This leads to significant reductions in the buckling capabilities of the booms. The Earth orbit's thermal load condition was used to calculate the temperature distributions and gradients of a single boom as shown in Fig. 10-11. The bending of the boom introduced by temperature gradients was then determined. The buckling capability of the bended boom was subsequently calculated to be 916 N. The baseline STR boom is capable of taking the required load, which is 156 N. Since the Earth application has the most severe thermal environment among all near-term mission applications, it was concluded that the STR booms

Fig. 10-9. 3-m Ka-band reflectarray membrane with 200,000 elements supported by two rigidizable inflatable tubes (shown on the right and left sides of the photo).

with current design and configuration are structurally strong enough for both near-Earth and deep-space applications in terms of buckling capability.

The thermally introduced deviation of the RF membrane is also investigated in this study. The case in which the antenna membrane aperture directly faces the Sun is identified as the worst situation because at that moment the inflatable antenna structure has the least moment of inertia to resist the thermal loads. The RF membrane deviations of the antenna, equipped with baseline STR booms, was analyzed. Figure 10-12 provides a rough illustration of how the bending occurs. The membrane tilt angle is calculated to be 0.758 deg, which is three times larger than the antenna beam-width (0.22 deg). This large tilt angle would lead to unacceptable degradation of RF performance and must be reduced. There are several ways to remedy this undesirable situation, including: (1) replacing steel spring tapes of the boom with composite spring tapes, since composite material is less sensitive to temperature change, (2) mechanically adapting the feed position to the membrane, and (3) electronically adapting the feed by using an array of feeds with a phase-compensation technique. However, replacing steel spring tapes of the boom with composite spring tapes is the most feasible and simplest way. To validate this, two antennas (one with the baseline STR booms and the other with booms that have their steel spring tapes replaced by composite tapes) were analyzed

Fig. 10-10. Rigidizable inflatable aluminum tubes reinforced by carpenter tapes. Right tube shows the end cap.

for thermal environments of the Earth, Mars, and Jupiter orbits. It was concluded from the results of these analyses that the current booms with steel tapes are not acceptable for Earth missions, but are acceptable for Mars and Jupiter missions. Conversely, the boom design with composite spring tapes is acceptable for all Earth, Mars, and Jupiter missions.

10.1.2.5 Recent Development of a 10-m Structure. It is envisioned that future inflatable antennas will not be limited to the size of 3 m as presented above. Sizes in the order of 5, 10, 20 m, etc., are likely to occur, depending on the distance that the spacecraft will travel and the needed data capacity. Analysis has shown that, each time the inflatable antenna size is increased approximately by twice, new challenges will be encountered. A new program was initiated in late 2004 to develop a larger inflatable reflectarray with a diameter in the order of 10 m. Several mechanical challenges are being studied. The most important one is the development of the 10-m long inflatable boom. This 10-m boom and its recent development are discussed in the following paragraph.

As the antenna aperture size increases, the strength of the inflatable booms also need to be increased in order to provide proper support and tensioning forces to the reflectarray surface. Analysis indicates that not only the boom diameter needs to be increased, the strength of the axial “carpenter” tapes also need to be enhanced by increasing either the tape size or its quantity. Furthermore, it was determined that in addition to these axial carpenter tapes, circumferential tapes are needed to enhance the boom’s strength in the non-

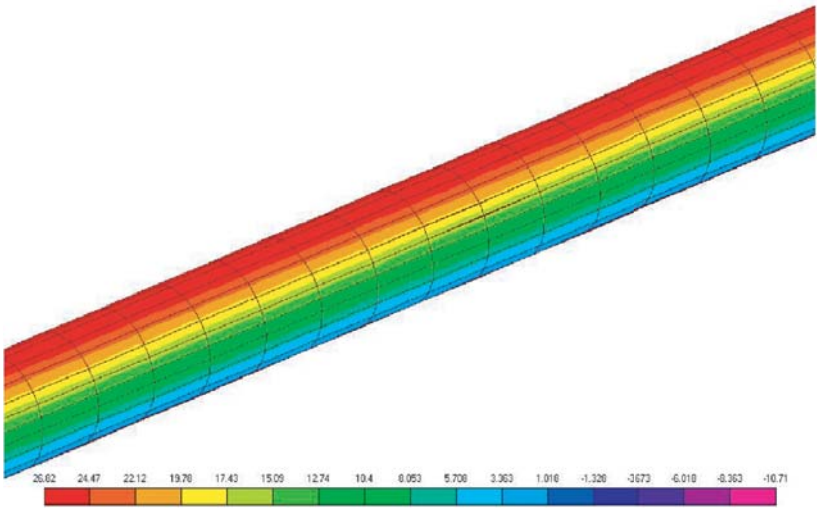

Fig. 10-11. Close-up view of temperature distribution of the 3.5-m inflatable boom. The dark color on top of the boom indicates the Sun's illumination with a temperature of 26.82 deg C, while the bottom of the boom's shadow region has a temperature of −10.71 deg C.

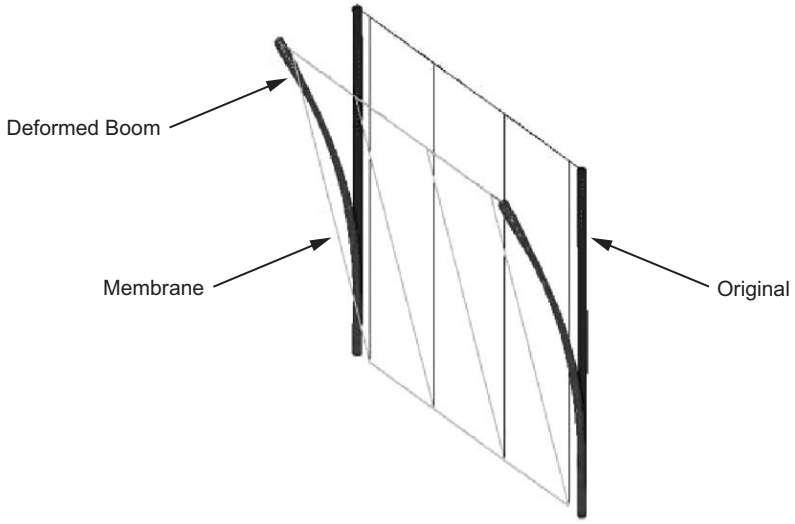

Fig. 10-12. Bending of the reflectarray membrane aperture due to thermally deformed inflatable booms.

axial direction so that buckling of the boom would not occur. This new boom structure, with both axial and circumferential tapes, is illustrated by a drawing and an actual photo in Fig. 10-13. Consequently, a 10-m long boom has been

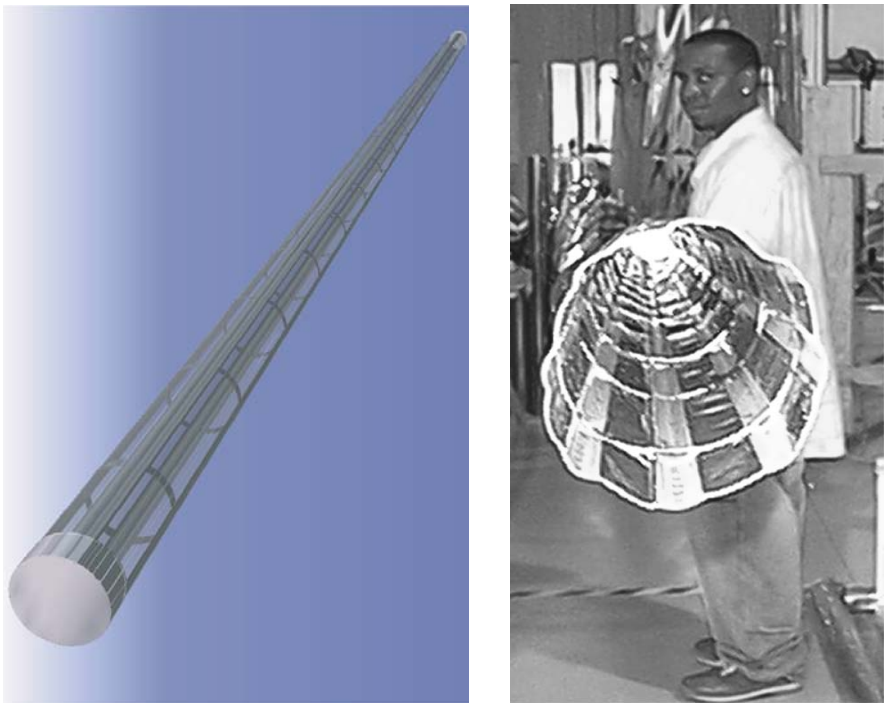

Fig. 10-13. Inflatable boom with axial and circumferential tapes.

constructed with rigidizable aluminum foil and both axial and circumferential tapes as shown in Fig. 10-14. This boom, having a diameter of 25 cm, will be tested under vibration to determine its mechanical resonant modes and strength. To carry out the vibration test under zero gravitational-force (0-g) effect, a special boom-support structure as shown in Fig. 10-14 was constructed. The 10-m long boom is hung along its length inside the support structure by many flexible bungee cords. A vibrating "gun" is used to hit one end of the boom horizontally. In this way, the boom will vibrate and show resonant modes in the horizontal direction with minimum g-force effect.

10.1.3 Technical Challenges for Inflatable Array Antennas

The above subsections presented two different types of inflatable arrays with each being a multilayer planar aperture surface that is supported and tensioned, through a catenary system, by several inflated tubular elements. In order to successfully develop these types of inflatable array antennas at any frequency throughout the microwave and millimeter-wave spectrums, several technical challenges must be addressed and resolved in the future. These challenges are separately discussed in the following subsections.

Fig. 10-14. 10-m inflatable boom and its support structure for vibration test.

10.1.3.1 Membrane Flatness and Separation. In order for a planar array to maintain certain required aperture efficiency and sidelobe/cross-polarization levels, the aperture membrane must maintain certain flatness accuracy. This required flatness, depending on the requirements, should generally be between

1/20th and 1/40th of a free-space wavelength. For a multilayer membrane aperture, specific membrane separation distances must also be maintained, especially for a microstrip array. If microstrip patches are separated with slightly different distances from their ground plane, they will resonate at different RF frequencies, which implies a very inefficient array aperture at the required operating frequency. Generally, the required membrane separation tolerance should be smaller than 1/20th of the absolute separation distance.

The above stringent flatness requirement is currently being addressed primarily by the tension force of the inflatable tube. The tighter the flatness requirement, the larger the tension force required, which implies that a larger inflation tube and stronger tube material are needed. All these will result in larger antenna mass, which is undesirable. The required membrane separation tolerance is currently met by, in addition to the tension force, using sparsely located small spacers. Tighter membrane separation tolerance implies that larger tension force and more spacers are needed, which also implies larger antenna mass. In the future, innovative techniques are needed for maintaining the required membrane flatness and layer separation without significantly increasing the antenna mass.

10.1.3.2 Inflatable Tube In-Space Rigidization Techniques. For any long-term space application, the inflatable tube needs to be rigidized once it is inflated in space. This is to avoid deflation and loss of tension force due to leaks in the inflatable structure or structures caused by impacting micrometeoriods and space debris. If the inflatable tubes are rigidized upon the completion of deployment, the need to carry a large amount of make-up gas to compensate for the leaks can thus be eliminated.

There are several rigidization techniques. One early technique was enabled by the development of several polymers that can be cured by space environments [11], such as vacuum, ultraviolet (UV) light, and cold temperature. A second technique is the use of stretched aluminum [12]. When thin aluminum foil is stretched by inflation pressure just above the aluminum's yield point, it rigidizes. Unfortunately, when the thin-wall aluminum tube becomes very long, it cannot carry large non-axial or bending loads. Aluminum with reinforced laminate material needs to be investigated. The third method is called hydro-gel rigidization [13], which uses woven graphite fabric impregnated with a water-soluble resin (hydro-gel). When evaporation of the water content occurs in space vacuum environment, the dehydrated gel fabric rigidizes to give structural stiffness. This rigidization technique, as well as the stretched aluminum, is a reversible process, which will allow several ground deployment tests prior to space flight. The fourth technique uses heat-cured thermoplastic material. Heating wires or electric resistive wires are imbedded into a soft plastic material, which rigidizes when heated to a certain

temperature. This curing process is also reversible; however, it may require a large amount of electric power depending on the size of the inflatable structure.

All the above techniques have certain advantages, as well as disadvantages. They require continued investigation and improvement. For each particular mission, their performance parameters, such as mass density, curing time, and bending stiffness, need to be subjected to a tradeoff study for selecting an optimal technique. Regardless of the rigidization technique, one major challenge is for the deployed structure to maintain its original intended structure shape and surface accuracy after rigidization.

10.1.3.3 Controlled Deployment Mechanism. In a space mission, there is a high probability that an uncontrolled inflation of a large inflatable structure might lead to self-entanglement, as well as damage to other spacecraft hardware. Thus, an inflatable antenna must be deployed in a well-controlled manner in both time and space domains. There are several controlled development mechanisms. One uses the compartmental valve control technique where the long inflatable tube is divided into a series of sectional compartments with a pressure-regulated valve installed at the beginning of each compartment. As the inflation gas enters, the tube gets sequentially deployed in a controlled manner. A second mechanism uses long coil springs, which are embedded along the inner walls of the inflatable tube. A controlled deployment of the tube is achieved by balancing the inflation pressure and the restoring force of the spring. The third technique is to use a long Velcro strip glued to the outside and along the long dimension of the tube wall. As the tube becomes inflated, the Velcro strip provides a certain amount of resistance force and thus achieves the controlled deployment. This technique, which already has space flight heritage, offers a significant advantage over the coil spring method because the Velcro strip, unlike the coil spring, will not impose any restoring force on the deployed tube when the inflation deployment is completed. The fourth technique of controlled deployment, proposed by L'Garde Corp., involves the use of a mandrel. During the deployment process, the inflation tube is forced to go over a guiding mandrel, which introduces a frictional force to balance the inflation pressure and to achieve the controlled deployment.

Research efforts should continue in the above controlled-deployment mechanisms, and improved or innovative concepts should be developed to minimize the mechanism's mass and risk impacts to the overall antenna system.

10.1.3.4 Packaging Efficiency. The inflation-deployment techniques currently used for array-type antennas are limited to the roll-up mechanism. No folding of the membrane is currently allowed in order to avoid the formation of large creases and cracks in the very thin copper traces on the membrane surface. Therefore, when the antenna is rolled up, its packaged minimum-achievable dimension is the short dimension of a rectangular aperture or the diameter of a

circular aperture. For examples, for a 10-m by 3-m aperture antenna, the packaged best-achievable dimension would be 3 m long. For a 10-m by 10-m aperture, the best-packaged dimension would be 10 m long, which can hardly fit into any current launch rocket. Therefore, it is imperative that innovative deployment techniques must be developed for future very large inflatable-array antennas.

10.1.3.5 Membrane Mountable Transmit/Receive (T/R) Modules. One of the major advantages of the inflatable-array antenna over that of the inflatable-reflector antenna is that the array antenna has the capability of achieving wide-angle beam scanning. To achieve beam scanning in both principle planes of a large array, many transmit/receive (T/R) amplifier modules with phase shifters need to be installed throughout the array aperture. Although current state-of-the-art technologies provide various miniaturized T/R modules, the packaged configurations of these modules, with significant mass and volume, preclude mounting onto the thin membrane surface. Very thin and low mass T/R modules should be developed in the future to preserve the beam-scanning capability of the array antenna. A very recent development of placing discrete amplifier and phase shifter components on thin membrane is to be presented in Section 10.3.

10.1.3.6 Modeling and Simulation of Static and Dynamic Space Environmental Effects. Inflatable antennas are a fairly new mechanical structure, and their structural form may vary significantly from one antenna to another. Accurate mathematical modeling and simulation techniques must be developed to predict the in-space static and dynamic effects for a variety of inflatable antenna types. Orbital and deep-space thermal effects, as discussed earlier, may distort the shape of the inflatable tubes or fatigue the aperture membranes. Spacecraft maneuvering will induce a natural vibration of the inflatable structure, which may also distort or damage the antenna. The effects of these static and dynamic forces on the inflatable structure need to be well understood through accurate calculation and/or simulation.

10.1.3.7 RF Design Challenges. Bandwidth performance is always an issue when an array antenna is involved. For example, with inflatable synthetic aperture radar (SAR) arrays, the technique of using series/parallel feed lines with good bandwidth for very large aperture antennas is still a challenging task. In the area of inflatable reflectarray, due to the use of phase delay lines, instead of time delay lines, bandwidth of more than 5 percent is very difficult to achieve. Dual-band or even triple-band reflectarray technology should be developed in the future to counter the bandwidth issue.

10.2 Foldable Frame-Supported Thin-Membrane Array

For Earth remote-sensing applications, a SAR typically employs an antenna with a fairly long along-track aperture in order to achieve the required resolution, swath width, and data rate. 10-m-long antennas, such as those for Seasat [14] and the SIR-A, -B, and -C [15] series, have been flown previously, and 50-m-long to 100-m-long apertures are being planned for the future. To maintain an acceptable electrical flatness across these long apertures, very massive antenna support and deployment structures have been and will be needed. For example, the fixed-beam L-band Seasat antenna, which used a microstrip array with a honeycomb substrate and 10-m × 3-m aperture, had a mass of 250 kg (including deployment mechanism). The electronic-beam-scanning L/C/X-band shuttle-based SIR-C antenna with similar aperture size is much heavier and had a mass of 1800 kg. These massive antenna systems generally require a launch vehicle with large stowage volume and heavy-payload-lift capability. On the other hand, in order to achieve high launch-volume efficiency and to reduce payload weight, low-mass inflatable array antennas are currently being developed as presented in the previous sections. However, it is unlikely that a beam-scanning inflatable phased array will be achieved in the near future prior to the availability of membrane-mountable electronics, T/R modules, and phase shifters. The concept presented in this section would achieve a deployable antenna with extreme light weight and, at the same time, have the capability of electronic beam scanning. This concept uses foldable low-mass rigid frames to support a set of multi-layer thin-membrane radiating apertures. The phase shifters and T/R modules can be rigidly mounted onto the frames. The frames are deployed by using the novel "carpenter tape" hinge, which is a simple, low cost, low mass, and reliable deployment and latching mechanism. With this foldable thin-membrane array concept [16], it is believed that Earth remote-sensing SAR antennas, in the near future, can achieve electronic beam scanning with low mass and large deployable apertures.

10.2.1 Antenna Description

The complete array antenna, with an aperture of 10 m × 2.85 m, would consist of 14 foldable panels that are made deployable by using the carpenter-tape hinges. Prior to deployment, these panels could be folded up to form a relatively small stowed volume of 2.85 m × 0.7 m × 0.9 m. In this development effort, instead of the full-size array, only a half array with 7 panels was fabricated and tested. This half array, shown in a photograph in Fig. 10-15, has a total radiating aperture of 5 m × 2.85 m. Each panel of this half array, sketched in Fig. 10-16, is a rectangular rigid frame that supports a two-layer, thin-membrane, L-band subarray aperture. The rigid frame is made of very low-

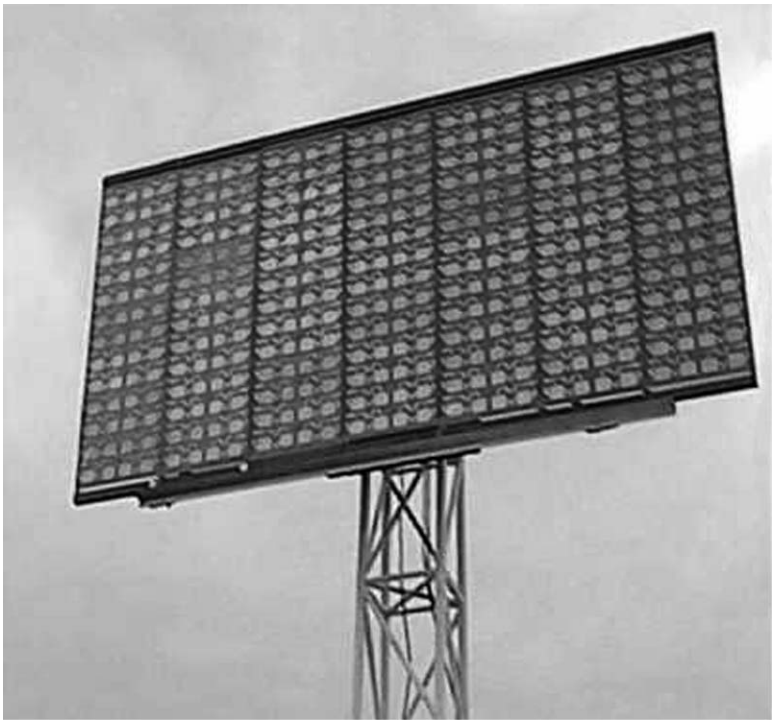

Fig. 10-15. Photograph of the half-size thin-membrane array with seven foldable panels, shown on a test fixture at an outdoor far-field range.

mass graphite composite material with honeycomb core and graphite epoxy face sheets. Each framed aperture has an aperture size of 2.85 m × 0.71 m and 14 rows of microstrip patch radiators with each row consisting of two 1 × 2 series-fed dual-polarized subarrays. The spacing between any two adjacent rows is 0.8 free-space-wavelength at the center operating frequency of 1.25 GHz. The spacing between adjacent patches in the horizontal direction is 0.74 free-space-wavelength. Each 1 × 2 subarray, as sketched in Fig. 10-16, can be connected to T/R modules that may be rigidly mounted onto the frame. The chief advantage of this "frame" concept is that each frame is able to rigidly support an appropriate number of T/R modules and phase shifters for achieving the desired beam scan. With this particular design, the complete array is able to scan its beam to ±20 deg in the vertical direction and a few degrees in the horizontal direction. In this development, however, T/R modules and phase shifters were not used, and all the 1 × 2 subarrays were connected together behind the ground plane via coax cables and discrete power dividers. For the two-layer thin-membrane structure, as shown in the photograph in Fig. 10-17, the top layer has all the radiating patches and microstrip transmission lines, while the bottom layer serves as the ground plane. Both layers are made of

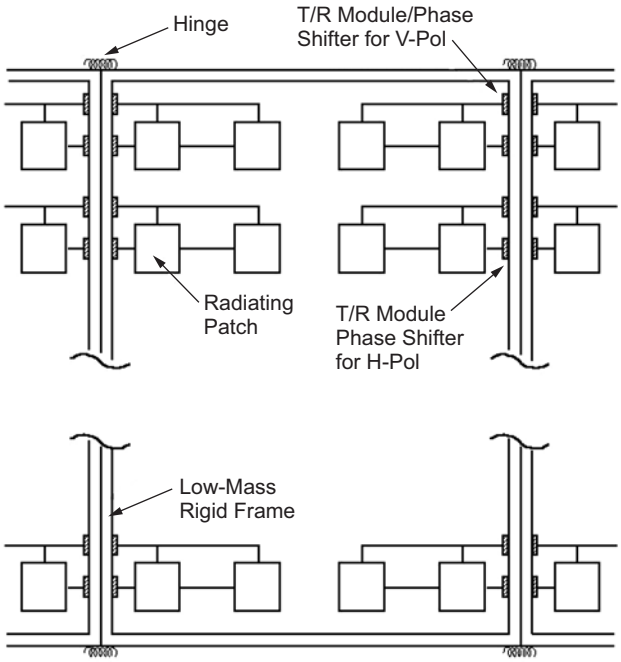

Fig. 10-16. Sketch of each framed panel with major components.

5-μm-thick copper deposited on 0.05-mm-thick Kapton membrane. The two layers are separated 1.3 cm apart for the purpose of achieving the required 80-MHz RF bandwidth.

To deploy the foldable panels, the novel but simple "carpenter tape" hinges were used. Figure 10-18 shows the carpenter tape hinge in its deployed and folded positions. Each hinge is comprised of two tape stacks with their concave side facing inward. Each of the stacks may have one to four layers of tapes. The tape hinge has two distinct performance regimes: When folded, it exhibits nonlinear behavior, with the ability to store significant amounts of energy in the tape deformation, which is released upon deployment. When latched after deployment, it acts as a rather stiff composite beam (linear behavior) to support the panels.

10.2.2 Antenna Performance Results

The half-size (5 m × 2.85 m) breadboard array antenna, shown in Fig. 10-15, was measured for its radiation characteristics at an outdoor far-field range. The typical measured patterns at 1.25 GHz for the vertically polarized array in both the E- and H-plane cuts are shown in Figs. 10-19 and 10-20, respectively. The peak sidelobe is about –12 dB, which is close to that expected

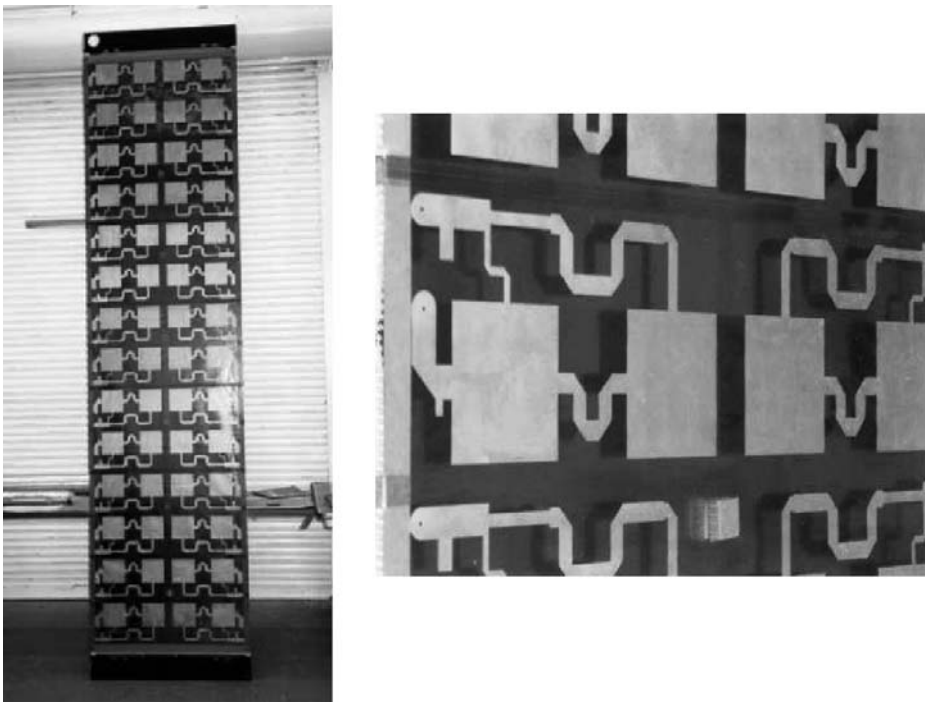

Fig. 10-17. Photographs of a single framed panel and a close-up view of the two-layer membrane patch elements.

for a uniformly distributed array. The cross-polarization lobes are mostly below –20 dB in the H-plane pattern, but they show –15 dB level in the E-plane. For SAR application, reduction of this –15 dB cross-polarization radiation to –20 dB level is needed in future development of this array. The measured 3-dB beamwidths in the E-plane and H-plane directions are 4.47 deg and 2.44 deg, respectively, which are very close to those expected for a uniformly distributed aperture of 2.85 m × 5 m. The input return losses measured at the inputs of the 1 × 2 subarray are below the required –10 dB level over a bandwidth of ±40 MHz centered at 1.25 GHz. The measured array efficiency (not including the losses of the coax cables and discrete power dividers) is 85 percent, which is considered quite good.

10.3 Thin-Membrane Array Antenna for Beam Scanning Application

An electronic beam scanning phased-array antenna with very large apertures (10 m to 100 m dimensions) will provide a wide range of radar capabilities for NASA's future Earth science missions, as well as deep-space planetary missions. For these very large arrays, the antenna mass, volume, and

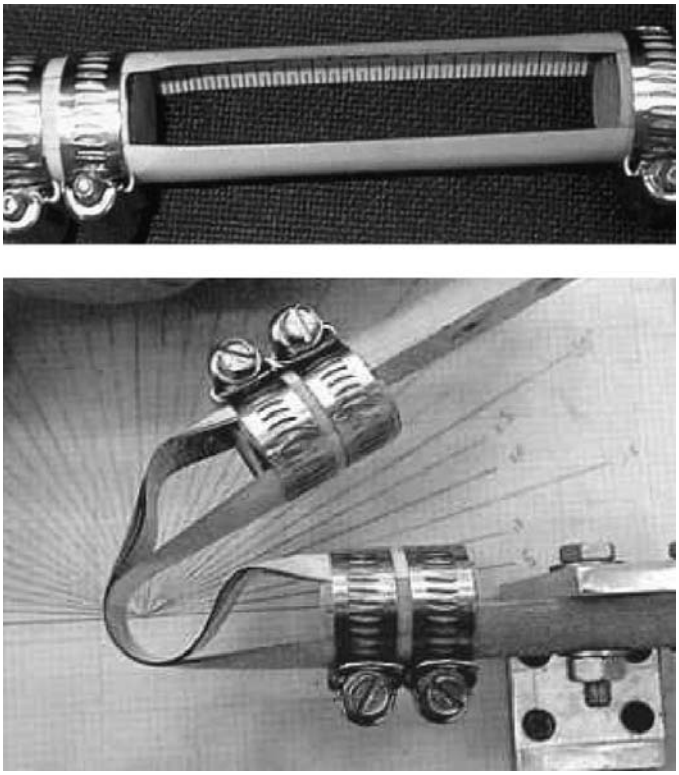

Fig. 10-18. The "carpenter tape" hinge.

cost will be prohibitive if the technology relies on previous rigid-panel phased arrays, such as the SIR-C antenna [17]. Previously developed membrane-based deployable passive array antennas [6] provided a means to reduce mass, launch-vehicle stowage volume, and overall cost compared to rigid antenna systems. However, to realize beam-scanning capability with thin-membrane-mounted active components, one of the challenges, as mentioned previously, is to develop T/R modules having the ability to integrate with thin-membrane patch arrays. The thin-membrane arrays must also be configured for easy integration with the T/R modules. As an initial effort, JPL has recently successfully developed a small L-band T/R-module-mounted thin-membrane array with 4×2 patch elements [18,19].

To avoid the use of many rigid coax feeding pins and associated solderings on thin membranes, aperture-coupling [7] is the ideal method for a large set of microstrip lines to feed a large array of microstrip patch elements. This aperture-coupling technique is employed here for the 4×2 array. Previously developed inflatable L-band array antennas [6] used three layers of thin

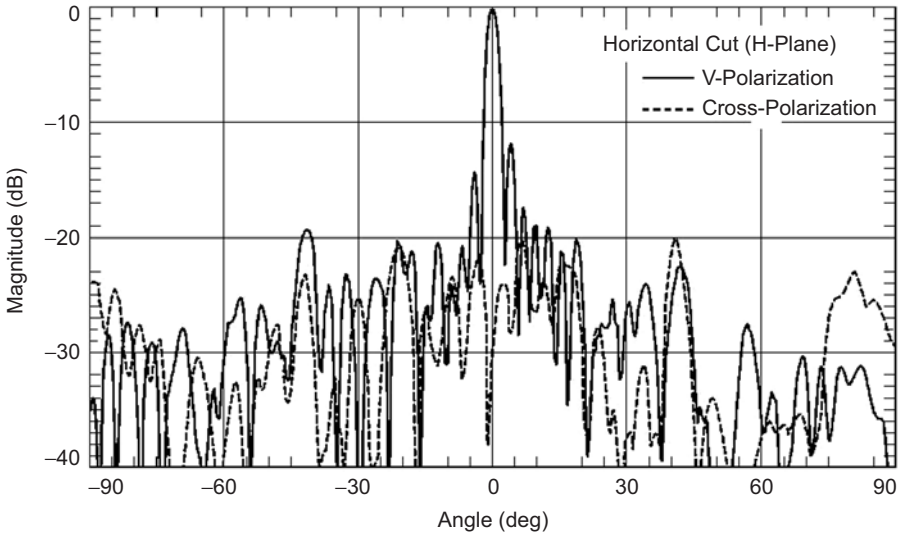

Fig. 10-19. Measured vertical-polarization pattern in the horizontal cut of Fig. 10-13.

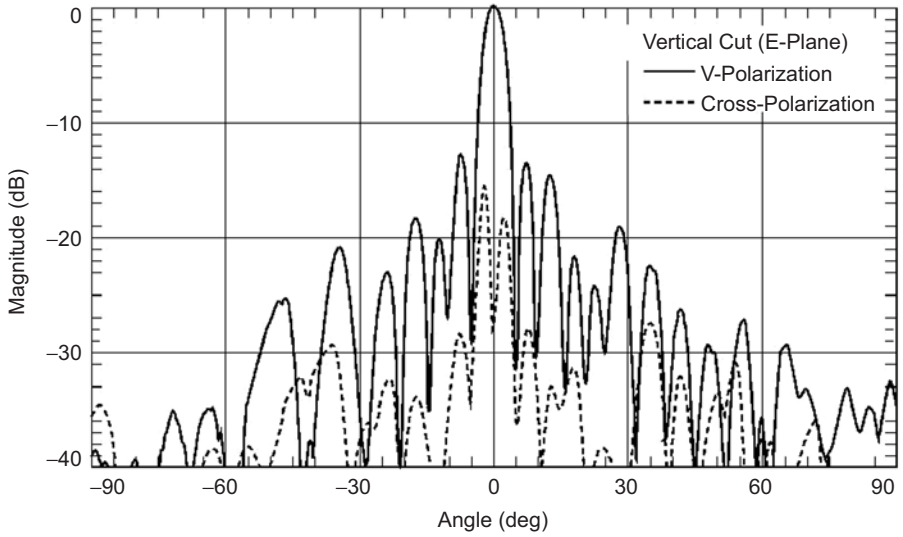

Fig. 10-20. Measured vertical-polarization pattern in the vertical cut of Fig. 10-13.

membranes as sketched in Fig. 10-21. These three layers, at the low microwave frequency of L-band, are separated with relatively large empty spaces of 0.64 cm and 1.27 cm. These large spaces make it difficult to integrate with small-size T/R modules, since small T/R modules with many electronic circuits

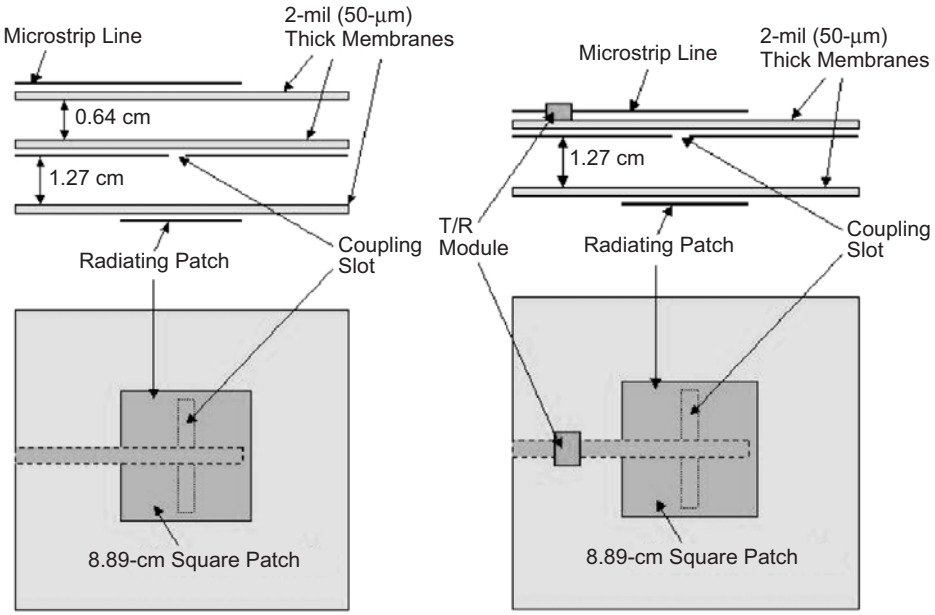

Fig. 10-21. Sketches of thin-membrane patch antennas. Left sketch is the previous three-layer approach; right sketch is the current two-layer approach.

function better with small separation distances from the ground plane. This development effort presents a new approach where only two thin-membrane layers are needed for the array elements. With this approach, as shown in Fig. 10-21, the top layer has both the microstrip lines and the slotted ground plane, while the bottom layer has only the patch elements. On the top layer, the microstrip lines are separated from the slotted ground plane via a very thin membrane substrate (0.05 mm). The microstrip line couples the energy to the patch through the slot in the ground plane. This approach allows easier integration with the membrane-based T/R modules where a single-layer co-planar waveguide (CPW) or microstrip transmission-line system is used [18]. This two-layer approach also allows the large-aperture antenna to be more easily rolled up with a smaller stowage volume than the previous three-layer system.

10.3.1 Antenna Description

Figure 10-22 shows the photograph of a single aperture-coupled membrane patch element with the left picture showing the bottom layer and the right picture showing the top patch layer. It can be observed that the coupling slot is very thin. It has dimensions of 79.5 mm by 0.48 mm with a length-to-width ratio of 160. The 4×2 array uses this same element design with linear polarization and an E-field parallel to the long dimension of the array. Two

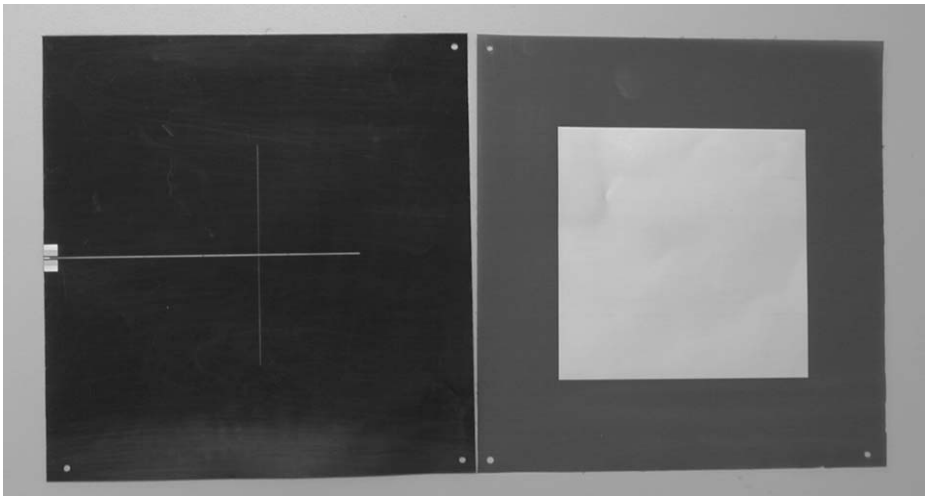

Fig. 10-22. Photograph of the single patch element showing two separated membrane layers.

4 × 2 arrays were fabricated and tested with one being a passive array and the other an active array. The active array is identical to the passive array except it has T/R modules integrated between the aperture-coupling slots and the power divider. Figure 10-23 gives both front and rear views of the 4 × 2 array, where the element spacing is 15.24 cm (0.64 λ_0) in both the vertical and horizontal planes. This spacing is selected to accommodate the T/R-module-required real estate while allowing the beam to scan to a relatively wide angle of 30 deg. Each patch is a square with a dimension of 8.89 cm and has a resonant frequency centered at 1.26 GHz. The array of elements is fed by a corporate microstrip power divider system with uniform amplitude distribution. The two membrane layers are each a 0.05-mm-thick polyimide material (Pyralux) having a relative dielectric constant of 3.4. On each membrane, the deposited copper is 5 μm thick. Both membranes are supported and tensioned by a framed catenary system to maintain the required membrane flatness (<5 mm rms) and membrane spacing (1.27 cm). The T/R module components, such as the amplifiers and phase shifters, are all commercially available devices. They are integrated onto JPL-designed membrane circuits. A close-up view of the T/R module circuitry is shown in Fig. 10-24 where it indicates that all components are small enough for the membrane to be rolled up.

10.3.2 Antenna Performance Results

The measured input return loss of the 4 × 2 passive array is given in Fig. 10-25 where it shows that the –10-dB return-loss bandwidth is about 100 MHz (8 percent) with a deep resonance occurring at 1.26 GHz. Due to the

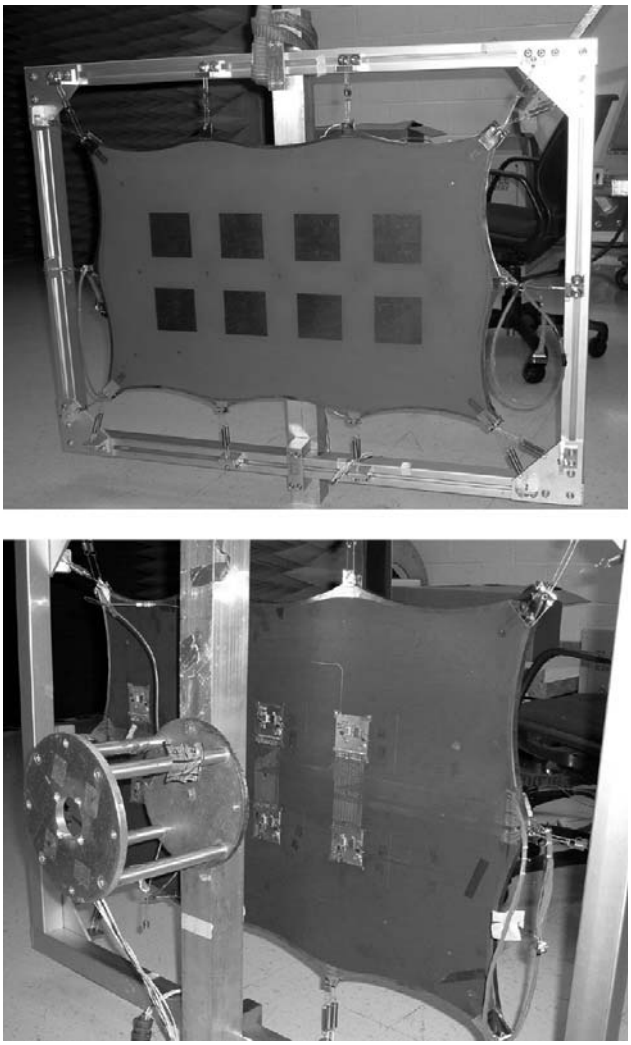

Fig. 10-23. Front (top) and rear (bottom) views of the 4 × 2 membrane array.

relative high loss material of the polyimide membrane substrate, the corporate power divider incurred a 2.5-dB insertion loss. The passive array achieved a measured gain of 12.1 dB (include the power divider loss). Both calculated and measured two-principal-plane radiation patterns at 1.26 GHz for 0-deg cut and 90-deg cut are shown in Fig. 10-26. The calculation was done by the moment-method-based Ensemble software. For the active array, the 4-bit phase shifters were adjusted for the main beam to scan to 15, 30, and 45 deg in the E-plane of the array. Both calculated and measured patterns for these three scanned beam

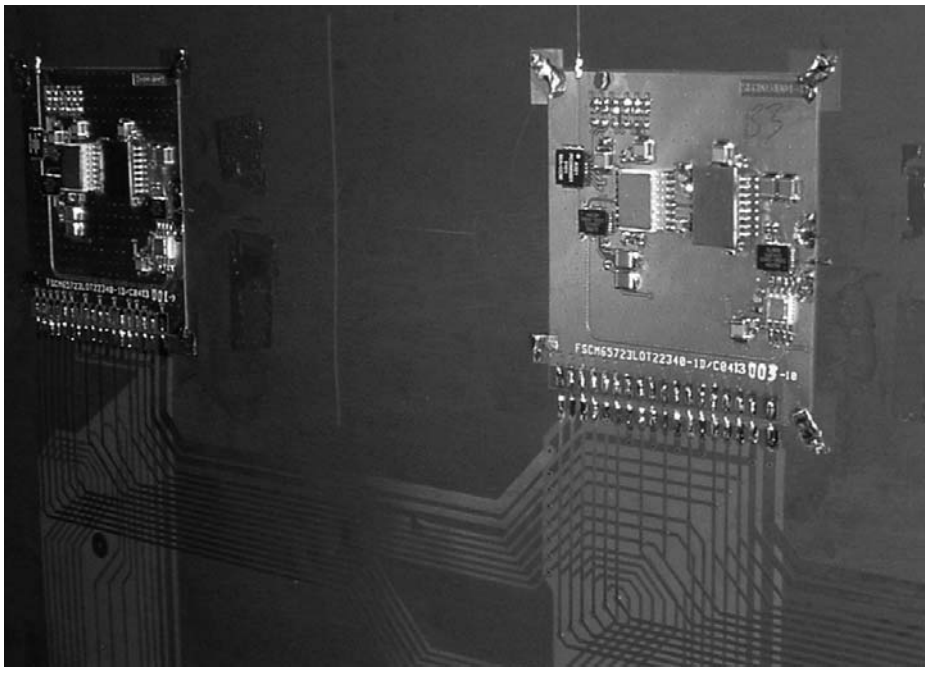

Fig. 10-24. Close-up view of the membrane array showing T/R module components.

positions are shown in Figs. 10-27, 10-28, and 10-29, respectively. The calculations agree well with the measured values. The 45-deg scanned beam has a significant drop in gain of about 3.0 dB. This is because, in order to achieve wide bandwidth with a relatively thick air substrate, the element pattern [19] formed a relatively narrow beam of ±42 deg, which suppresses the array's 45-deg-scanned beam. In addition, due to the element spacing of 0.64 λ_0, the grating lobe starts to form, which further reduces the main beam gain. Nevertheless, the 4×2 active array has successfully demonstrated that the membrane-based beam-scanning array is very feasible.

10.4 Printed Reflectarray Antenna

Since the printed reflectarray is a fairly new antenna concept, this section gives a more detailed discussion and an overview of the development history and key design methodologies for this antenna. The reflectarray antenna consists of a flat or slightly curved reflecting surface and an illuminating feed as shown in Fig. 10-30. On the reflecting surface, there are many isolated elements (e.g., open-ended waveguides, printed patches, dipoles, or rings) without any power division transmission lines. The feed antenna illuminates these isolated elements, which are designed to scatter the incident field with

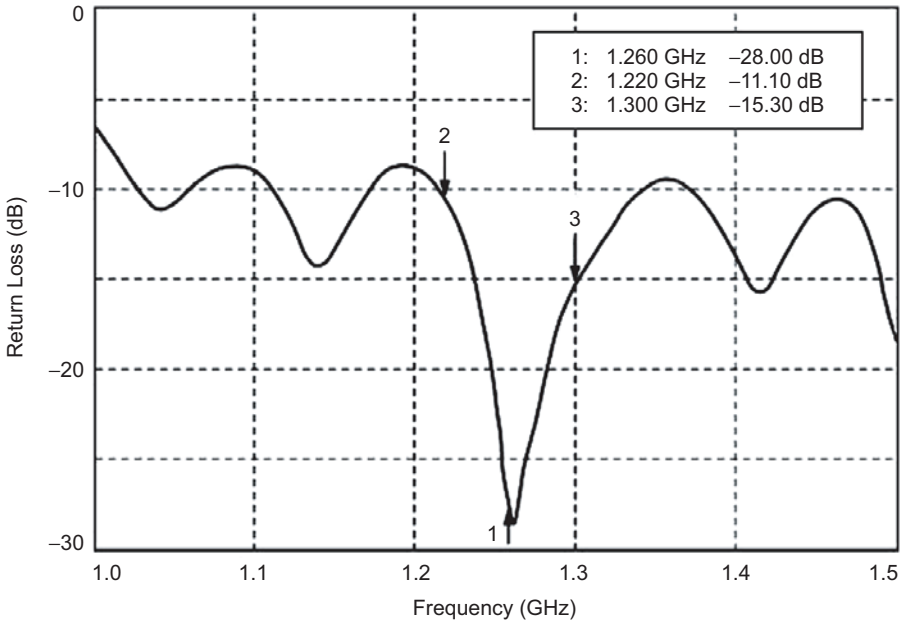

Fig. 10-25. Measured input return loss of the 4 × 2 membrane passive array.

electrical phases that are required to form a planar phase front in the far-field distance. This operation is similar in concept to the use of a parabolic reflector that naturally reflects and forms a planar phase front when a feed is placed at its focal point. Thus, the term "flat reflector" is sometimes used to describe the reflectarray, which utilizes both technologies of reflector and array. As shown in Fig. 10-31, there are several methods for reflectarray elements to achieve a planar phase front. For example, one is to use identical microstrip patches with different-length phase-delay lines attached so that they can compensate for the phase delays over the different paths from the illuminating feed. The other is to use variable-size patches, dipoles, or rings so that elements can have different scattering impedances and, thus, different phases to compensate for the different feed-path delays. The third method, for circular polarization only, the reflectarray has all identical circularly polarized elements but with different angular rotations to compensate for the feed path length differences.

10.4.1 Advantages/Disadvantages of Printed Reflectarrays

To achieve a low-reflecting surface profile and a low antenna mass, reflectarrays using printed microstrip elements have been developed. These reflectarrays combine some of the best features of the traditional parabolic reflector antenna and the microstrip-array technology. As with the parabolic reflector, the reflectarray can achieve very good efficiency (>50 percent) for

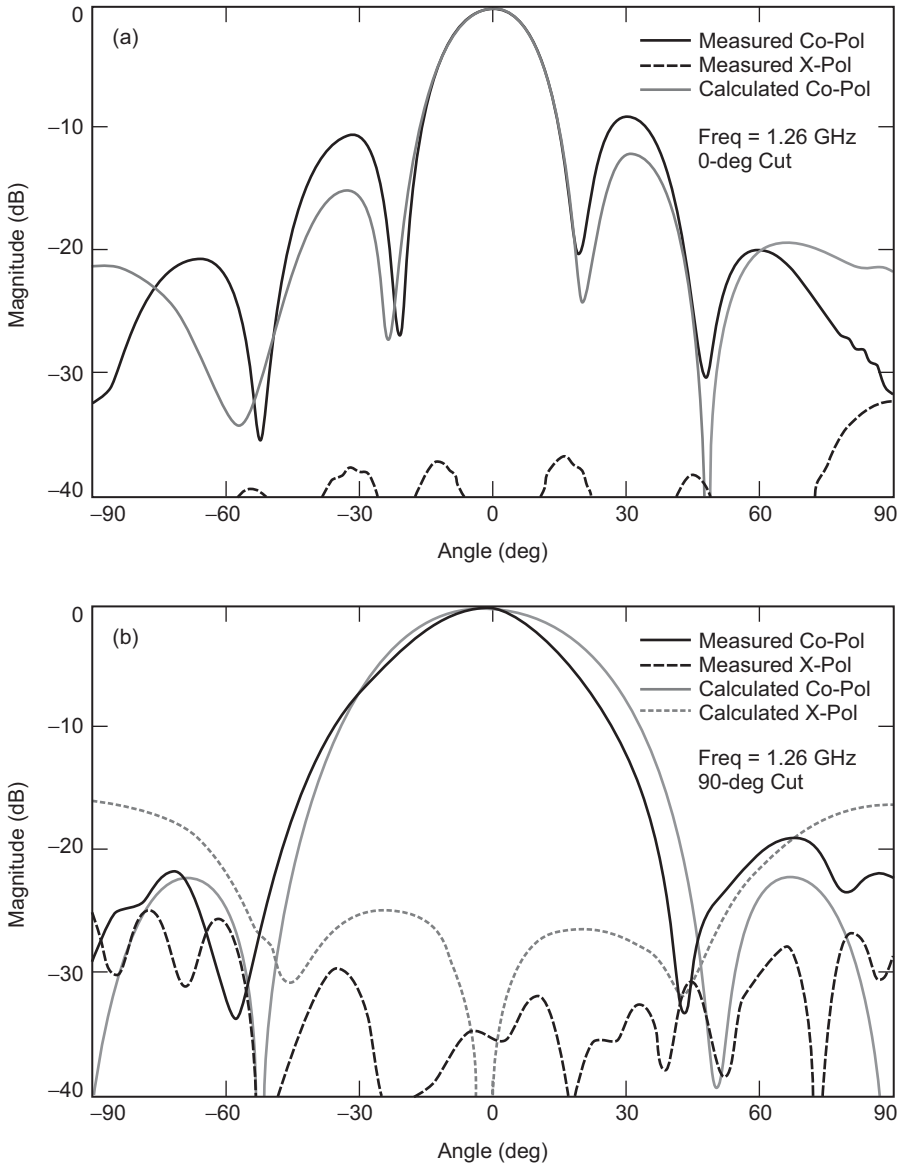

Fig. 10-26. Two-principal-plane patterns of the 4 × 2 membrane passive array radiation patterns for (a) 0-deg cut and (b) 90-deg cut.

very large aperture since no power divider is needed and thus very little resistive insertion loss is encountered here. On the other hand, very similar to an array antenna, the reflectarray can have its main beam designed to tilt at a large angle (>50 deg) from its broadside direction. Low-loss electronic phase

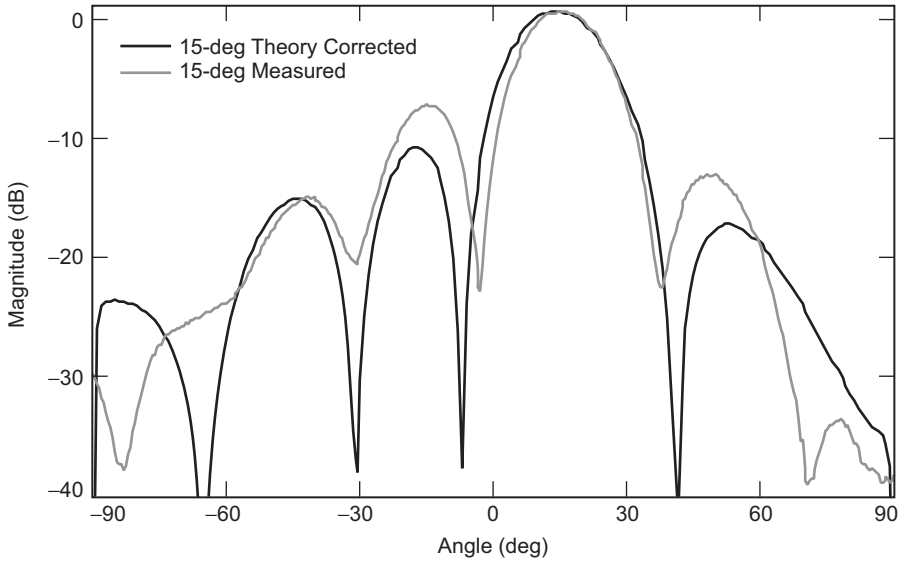

Fig. 10-27. 15-deg scanned pattern of the 4 × 2 active array.

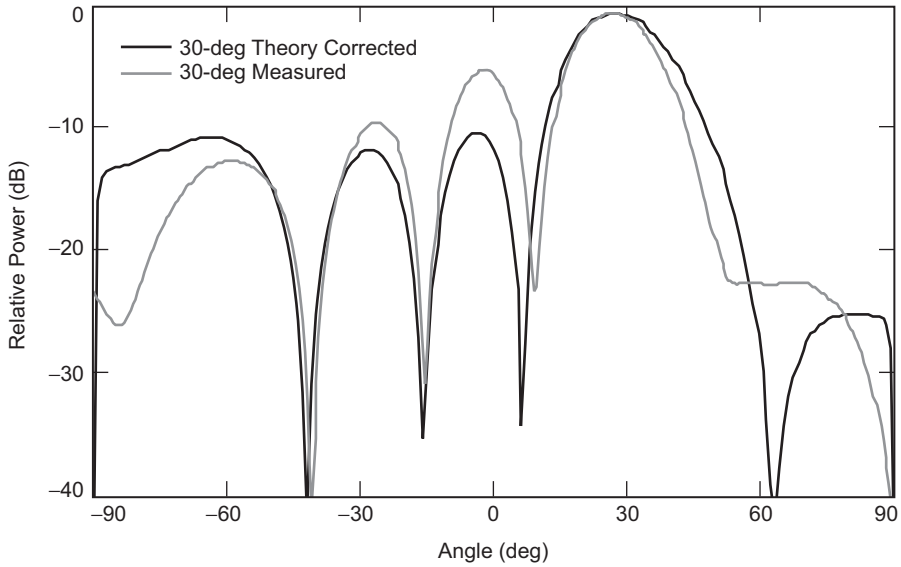

Fig. 10-28. 30-deg scanned pattern of the 4 × 2 active array.

shifters can be implanted into the elements for wide-angle electronic beam scanning. With this beam scanning capability of the reflectarray, the complicated high-loss beamforming network and high-cost transmit/receive

(T/R) amplifier modules of a conventional phased array are no longer needed. One significant advantage of the printed reflectarray is that, when a large aperture (e.g., 10-m size) spacecraft antenna requires a deployment mechanism, the flat structure of the reflectarray allows a much simpler and more reliable

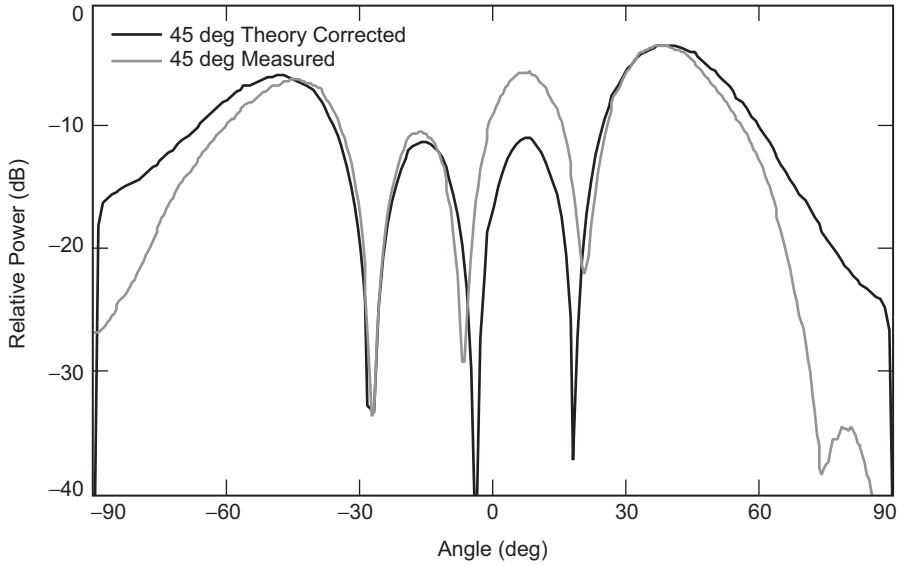

Fig. 10-29. 45-deg scanned pattern of the 4 × 2 active array.

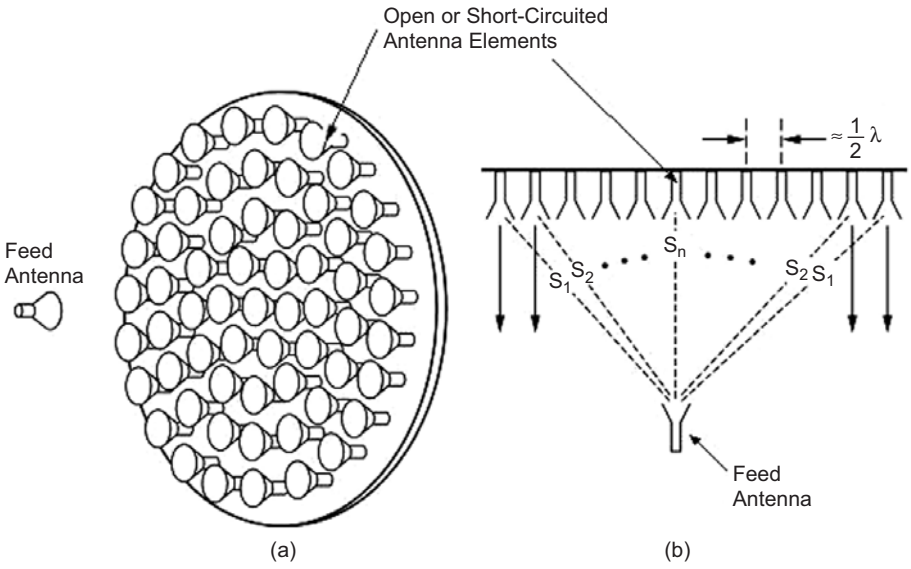

Fig. 10-30. Configuration of a reflectarray antenna in (a) three-dimensional view and (b) two-dimensional view.

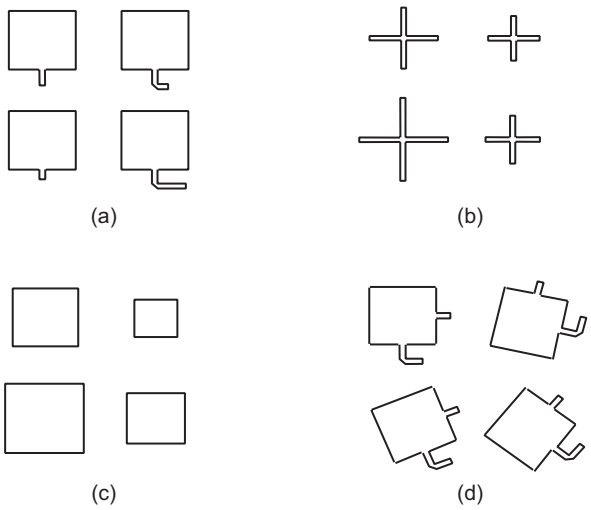

Fig. 10-31. Various reflectarray elements: (a) identical patches with variable-length phase delay lines; (b) variable-size dipoles; (c) variable-size patches; (d) variable angular rotations.

folding or inflation mechanism than the curved surface of a parabolic reflector. The flat reflecting surface of the reflectarray also lends itself to flush mounting onto an existing flat structure without adding significant mass and volume to the overall system structure. The reflectarray, being in the form of a printed microstrip antenna, can be fabricated with a simple and low-cost etching process, especially when produced in large quantities. Another major feature of the reflectarray is that, with hundreds or thousands of elements in a reflectarray having phase adjustment capability, the array can achieve very accurate contour beam shape with a phase synthesis technique. With all the above capabilities, there is one distinct disadvantage associated with the reflectarray antenna. This is its inherent narrow bandwidth, which generally cannot exceed much beyond ten percent. This narrow bandwidth behavior is discussed further in 10.4.4 Although the reflectarray has narrow bandwidth, due to its multitude of capabilities, the development, research, and application of the printed reflectarray antenna would be boundless in the future.

10.4.2 Review of Development History

The reflectarray antenna concept, shown in Fig. 10-30, was first demonstrated during the early 1960s [20]. Open-ended waveguide elements with variable-length waveguides were used to demonstrate the capability of achieving co-phasal re-radiated far-field beams. Since, during this early time, most wireless operations were done at relatively low microwave frequencies,

the large-waveguide reflectarrays resulted in very bulky and heavy antennas. In addition, the efficiencies of these reflectarrays were not studied and optimized. More than ten years later (in the mid 1970s), the very clever concept of the "spiraphase" reflectarray was developed [21], in which switching diodes were used in an eight-arm spiral or dipole element of a circularly polarized reflectarray to electronically scan its main beam to large angles from the broadside direction. This is possible because, by angularly rotating a circularly polarized radiating element, its propagating electrical phase will also change by an amount proportional to the amount of rotation. However, due to the thick spiral cavity and large electronic components, the spiraphase reflectarray was still relatively bulky and heavy. Its aperture efficiency was still relatively poor. Thus, no continued development effort was followed. It should be noted here that, in order to have good efficiency for the reflectarray, the intricate relations between the element phasing, element beamwidth, element spacing, and focal length/diameter (f/D) ratio must be well designed; otherwise, a large backscattered component field or a mismatched surface impedance would result.

Due to the introduction of the printable microstrip antennas, the technologies of reflectarray and microstrip radiators were combined, and a typical configuration is illustrated in Fig. 10-32. Various printed microstrip reflectarray antennas were developed in the late 1980s and early 1990s for the purpose of achieving reduced antenna size and mass. These printed reflectarrays came in various forms, as shown in Fig. 10-31, but all have flat low-profile and low-mass reflecting surfaces. The reflectarrays that used identical patch elements with different-length phase delay lines [22–27] have

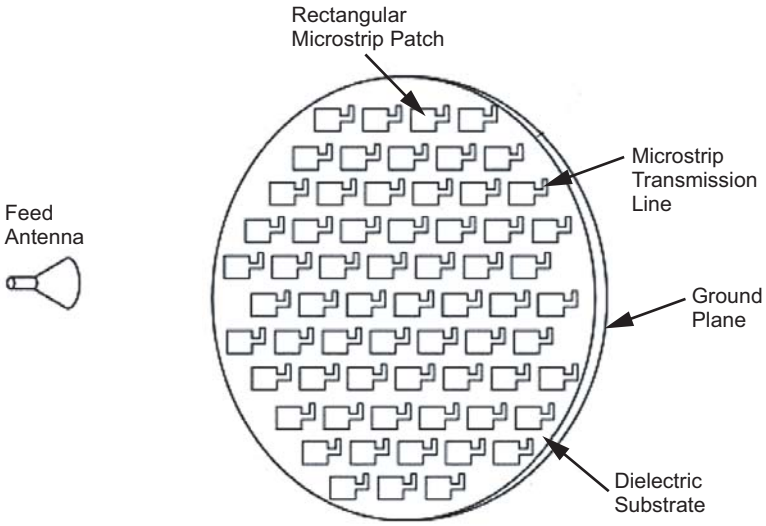

Fig. 10-32. Configuration of printable microstrip reflectarray antenna.

their elements similar to those shown in Fig. 10-31(a). The phase delay lines, having lengths on the order of a half-wavelength long or less, are used to compensate for the phase differences of different path lengths from the illuminating feed. The second approach, shown in Fig. 10-31(b), used elements that are made of printed dipoles with variable dipole lengths [28]. Different dipole lengths yield different scattering impedances, which then provide the different phases needed to compensate for the different path-length delays. Similarly, microstrip patches with variable patch sizes [29], shown in Fig. 10-31(c), were also developed. Circularly polarized microstrip patches with identical size but variable angular rotations [8,30], shown in Fig. 10-31(d), were designed to form a co-phasal far-field reflectarray beam. In addition to those shown in Fig. 10-31, several other reflectarray or equivalent developments during the 1990s are worth mentioning here. Printed variable-length dipole elements were used to form a frequency-scanned grating-reflector antenna with an offset feed [31]. Printed annular rings of variable diameters arranged in Fresnel zone configuration were also used to focus the beam [32]. In the 1996 Phased Array Conference, a 94-GHz monolithic reflectarray [33], using a 1-bit p-type, intrinsic, n-type (PIN) diode phase shifters, was reported to achieve wide-angle (±45 deg) electronic beam scanning. In the same conference, a 35-GHz reflectarray, using waveguide/dielectric elements with 3-bit ferrite phase shifters [34], was also reported to achieve ±25-deg beam scanning. One proposed technique [30], although not yet developed, is worth mentioning here. By using the angular rotation technique with circularly polarized elements, miniature or micro-machined motors could be placed under each element to achieve wide-angle beam scanning without the need of T/R modules and phase shifters. For application in the spacecraft area, a deployable and low-mass 1-meter diameter inflatable reflectarray antenna [35] at the X-band frequency was developed. Another unique spacecraft application of the reflectarray was conceived [36] and developed [37] by using its many elements, with a numerical phase synthesis technique, to form a uniquely shaped contour beam. From all the above developments, it can be seen that, at the beginning of the Twenty-First Century, the reflectarray antenna technology is becoming mature enough and has a variety of possible applications throughout the microwave and millimeter-wave spectra.

By early 2000, the development of reflectarray had mushroomed and several performance improvement techniques are worth mentioning here. One used multi-layer stacked patches to improve the reflectarray bandwidth from a few percent to more than ten percent [38]. As an extension to the 1-m X-band inflatable reflectarray mentioned above, a 3-m Ka-band inflatable reflectarray consisting of 200,000 elements was also developed [39], which is currently known as the electrically largest reflectarray. An amplifying reflectarray was developed [40] for each element of the reflectarray to amplify the transmitted signal and, thus, achieving very high overall radiated power. In order to achieve

good antenna efficiency, the most critical segment of the reflectarray design is its elements. The element performance was optimized by using the genetic algorithm technique [41]. The reflectarray using a subreflector and array feed configuration to achieve fine beam scanning was also studied [42]. To combat the shortcoming of narrow bandwidth, dual-band multi-layer reflectarrays using annular rings [43] and crossed dipoles [44] are also being developed. Another development that is worth mentioning here is a folded reflectarray configuration [45], where two reflecting surfaces are used to reduce the overall antenna profile due to the feed height of a conventional reflectarray.

10.4.3 Analysis and Design Procedures

The design and analysis of a reflectarray can be separated into four essential steps, which are separately discussed below:

10.4.3.1 Element Characterization. The most important and critical segment of the reflectarray design is its element characterization. If the element design is not optimized, it will not scatter the signal from the feed effectively to form an efficient far-field beam. Its beamwidth must correlate correctly with the reflectarray's f/D ratio to accommodate all incident angles from the feed. Its phase change versus element change (patch size, delay line length, etc.) must be calibrated correctly. One of the most popular techniques to calibrate the phase is to use the infinite-array approach [29,46] to include local mutual coupling effects due to surrounding elements. It is not yet feasible for computers to provide a complete rigorous solution including all the mutual coupling effects of all elements since the reflectarray generally consists of too many elements. The infinite array approach can be done by using the method of moment technique [29,46] or equivalently done by a finite-difference time-domain (FDTD) analysis on a unit cell of a single element [47]. A mathematical waveguide simulator, which simulates the infinite array approach, can also be adapted by using the commercial software—HFSS (a finite element technique) to achieve the element-phase information. All these techniques are used to derive the phase-versus-element-change curve, which is generally an S-shaped curve with nonlinear relationship, as illustrated in Fig. 10-33. The antenna designer should minimize the slope at the center of the curve so that the phase change will not be overly sensitive to the element change. If the curve is too steep, the element change or fabrication tolerance may become an issue, in particular at high microwave frequencies.

10.4.3.2 Required Phase Delay. The path lengths from the feed to all elements are all different, which lead to different phase delays. To compensate for these phase delays, the elements must have corresponding phase advancements designed in according to a unique S-curve similar to that shown in Fig. 10-33.

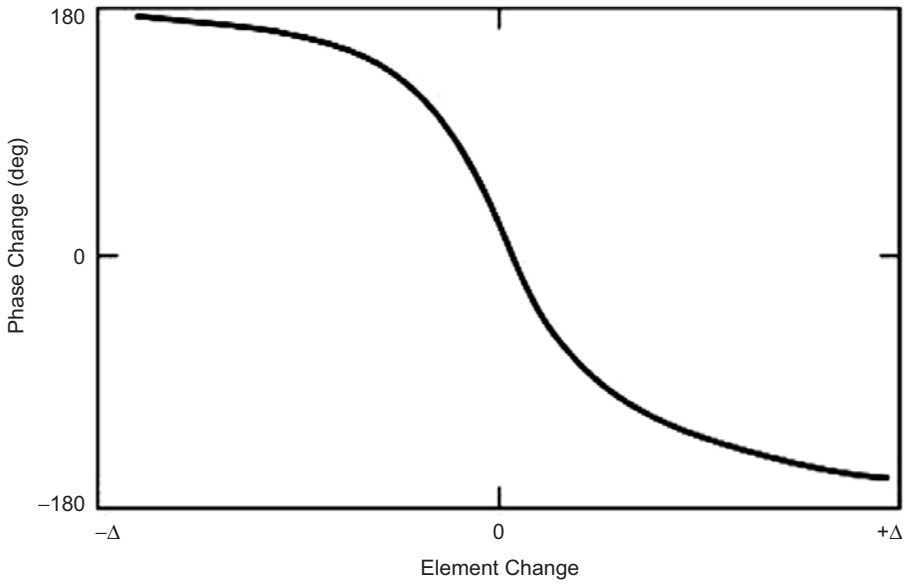

Fig. 10-33. A typical S-curve of a reflectarray element phase-change versus element-change.

The following gives an example of how the compensating phase is calculated for each element of a reflectarray with a broadside-directed beam. The differential path length for each element is given as:

$$\Delta L_{m,n} = L_{m,n} - L_{0,0} \tag{10.4-1}$$

where:

$L_{m,n}$ = distance between the feed and the *mn*-th element, which can be obtained by using simple geometry;

$L_{0,0}$ = distance between the feed and a reference point on the reflectarray surface (e.g., the center point).

$\Delta L_{m,n}$ = differential feed path length for the *mn*-th element.

To achieve a collimated radiation, the phase advancement $\Delta\Phi_{mn}$ needed for the *mn*-th element is given by

$$\Delta\Phi_{mn} \text{ in degrees } = \left[\frac{\Delta L_{m,n}}{\lambda_0} - \text{integer of}\left(\frac{\Delta L_{m,n}}{\lambda_0}\right)\right] \times 360 \tag{10.4-2}$$

The above indicates that the compensating phase can be repeated every 360 deg, and the portion that is an integer multiple of a wavelength or 360 deg can be deleted.

10.4.3.3 Pattern Calculation. With the compensating phases of all elements known, the far-field radiation patterns can be calculated by the conventional array theory [48], where the radiations of all elements are summed together as follows. Consider a planar array consisting of $M \times N$ elements that are non-uniformly illuminated by a low-gain feed at position vector $\vec{r}_f$. Let the desired beam direction be specified by unit vector $\hat{u}_0$. Then, the far field of the reflectarray in the direction will be of the form:

$$E(\hat{u}) = \sum_{m=1}^{M} \sum_{n=1}^{N} F\left(\vec{r}_{mn} \bullet \vec{r}_f\right) \cdot A\left(\vec{r}_{mn} \bullet \hat{u}_0\right) \cdot A\left(\hat{u} \bullet \hat{u}_0\right) \cdot \exp\left[jk\left(\left|\vec{r}_{mn} - \vec{r}_f\right| + \vec{r}_{mn} \bullet \hat{u}\right) + j\alpha_{mn} \right] \tag{10.4-3}$$

where F is the feed pattern function, A is the reflectarray element pattern function, $\vec{r}_{mn}$ is the position vector of the mn-th element, and α_{mn} is the required compensating phase of the mn-th element calculated by Eq. (10.4-2). $\cos^q \theta$ factor is used for both F and A functions with no azimuth (φ) dependence.

10.4.3.4 Reflectarray Geometry Design. To determine the geometry of a reflectarray is basically to determine its f/D ratio, which is governed by its desired aperture efficiency. The aperture efficiency (η_a) can be defined as the product of the illumination (η_I) and spillover (η_s) efficiencies: $\eta_a = \eta_I \times \eta_s$. By integrating the pattern function of Eq. (10.4-3), the illumination efficiency for a center-fed reflectarray can be obtained in a close form [48] as given by

$$\eta_I = \frac{\left[\dfrac{1 + \cos^{q+1} \theta_e}{q+1} + \dfrac{1 - \cos^q \theta_e}{q} \right]^2}{2 \tan^2 \theta_e \dfrac{1 - \cos^{2q+1} \theta_e}{2q+1}}, \tag{10.4-4}$$

and the spillover efficiency is given by

$$\eta_s = 1 - \cos^{2q+1} \theta_e \tag{10.4-5}$$

where q is the exponent of the feed pattern function represented by $\cos^q \theta$ and θ_e is half of the subtend angle from the feed to the reflectarray aperture. The

reflectarray element is approximated by the cosine function. Equations (10.4-4) and (10.4-5) are calculated by assuming a circular aperture only for the demonstration of the design procedures. Similar closed-form equations can be easily obtained for square, rectangular, or elliptical apertures by performing proper integrations. To give an example about how Eqs. (10.4-4) and (10.4-5) can be utilized to optimize a reflectarray design, Fig. 10-34 shows the calculated curve of spillover and illumination efficiencies versus the feed pattern factor q (feed beamwidth) for a half-meter 32-GHz reflectarray with a fixed f/D ratio of 1.0 ($\theta_e = 26.6$ deg). It demonstrates that the maximum aperture efficiency is achieved at $q = 10.5$ or when the feed has a –3-dB beamwidth of 29 deg. Another curve, shown in Fig. 10-35, gives aperture efficiency as a function of f/D ratio for the same half-meter 32-GHz reflectarray when the feed beamwidth is fixed at 33.4 deg with $q = 8$. In this case, the maximum aperture efficiency is achieved when the f/D ratio is 0.87. It can be seen that curves derived from Eqs. (10.4-4) and (10.4-5) are essential in obtaining an optimum efficiency design. The above discussion has been limited to center-fed reflectarray. Offset reflectarrays can also be optimally designed by using equations similar to Eqs. (10.4-4) and (10.4-5).

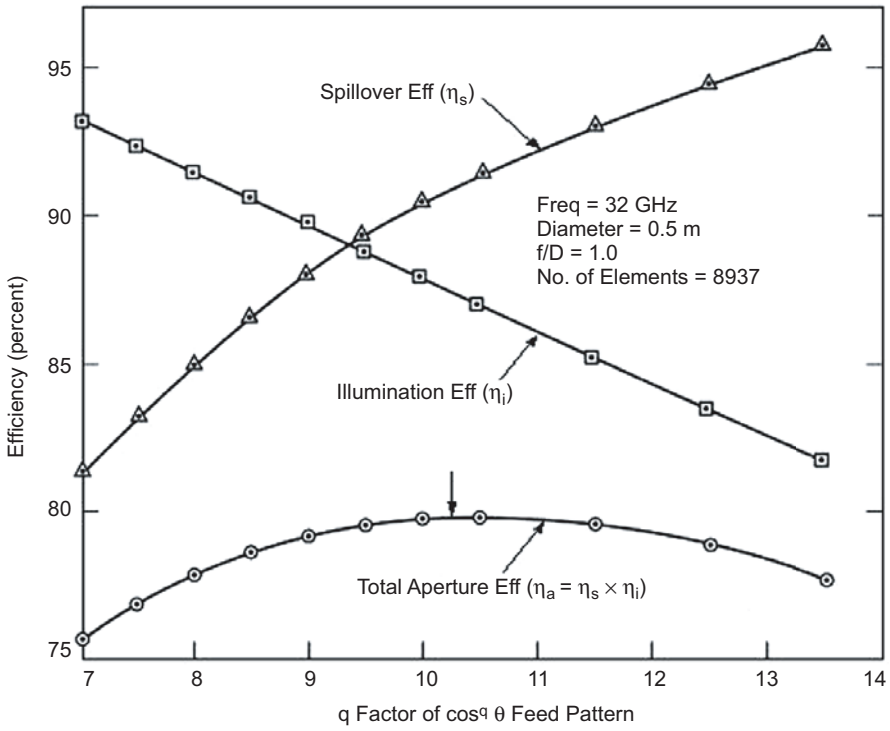

Fig. 10-34. Spillover and illumination efficiencies versus feed pattern shape.

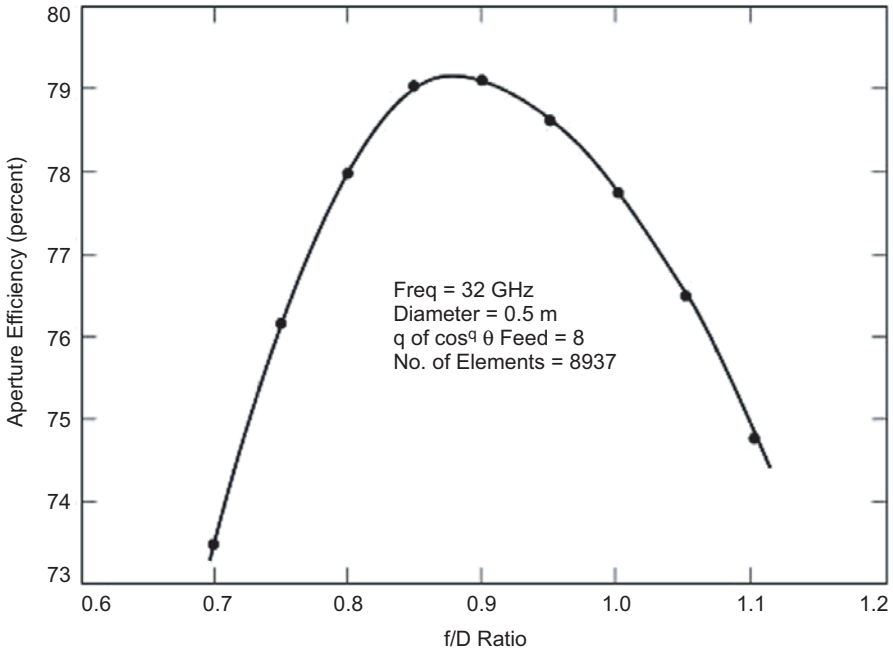

Fig. 10-35. Aperture efficiency versus f/D ratio.

10.4.4 Bandwidth Issues

The bandwidth performance of a reflectarray [30] is no match for that of a parabolic reflector, where theoretically infinite bandwidth exists. For a printed microstrip reflectarray, its bandwidth is primarily limited by two factors. One is the narrow bandwidth of the microstrip patch elements on the reflectarray surface, and the other is the differential spatial phase delay. The microstrip patch element generally has a bandwidth of about 3 to 5 percent. To achieve wider bandwidth for a conventional microstrip array, techniques such as using thick substrate for the patch, stacking multiple patches, and using sequentially rotated subarray elements have been employed. Bandwidths greater than 15 percent have been reported. The second reflectarray-limiting factor, the differential spatial phase delay, can be best explained by referring to Fig. 10-36 where the differential spatial phase delay, ΔS, is the phase difference between the two paths S_1 and S_2 from the feed to the reflectarray elements. This ΔS can be many multiples of the wavelength (λ) at the center operating frequency. It can be expressed as $\Delta S = (n + d)\lambda$ where n is an integer and d is a fractional number of a free-space wavelength λ. At each element location, d is compensated by an appropriate phase delay achieved by the reflectarray element design (achieved by variable patch size, variable phase delay line length, etc.). As frequency changes, the factor $(n + d)\lambda$ becomes $(n + d)(\lambda + \Delta\lambda)$. Since the design and the compensating phase for each element is fixed

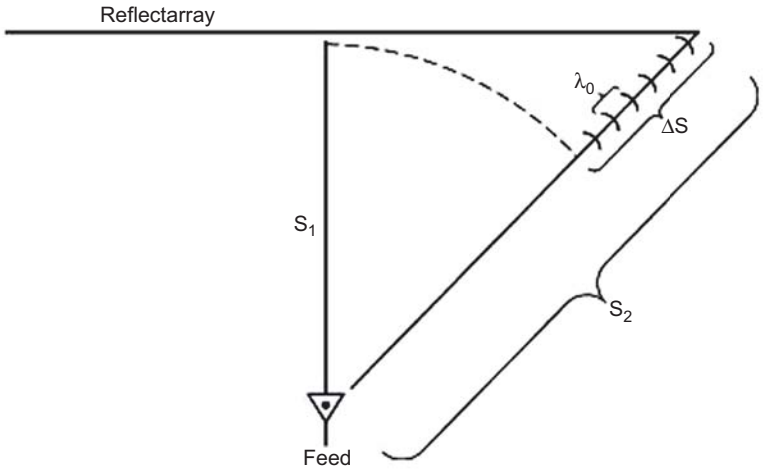

Fig. 10-36. Differential spatial phase delay limits the bandwidth of a reflectarray.

for the center frequency, a frequency excursion error will occur in the re-radiated phase front. The amount of phase change in each path when compared to a reference path, say S_1, is $(n + d)\Delta\lambda$, which can be a significant portion of a wavelength or 360 deg.

To reduce the amount of frequency excursion error mentioned above, the integer number n must be reduced. There are several methods to reduce n. One is to design the reflectarray with a larger f/D ratio and hence to minimize the difference between paths S_1 and S_2. The second way is simply to avoid the use of a reflectarray with a large electrical diameter. The effect of f/D ratio on bandwidth performance was given previously in Fig. 10-35. The third method to reduce frequency excursion error is to use time-delay lines or partial-time-delay lines instead of the phase delays. In other words, when using the phase delay line technique (not the variable patch size technique), instead of using $d\Delta\lambda$ for the delay line length, $(n + d)\Delta\lambda$ could be used for the delay line. Certainly, additional line-insertion loss and needed real estate for the lines are issues to be encountered. Another method to increase the bandwidth is to use, instead of a complete flat reflectarray surface, a concavely curved reflectarray with piecewise flat surfaces. This curved reflectarray has advantages over a curved parabolic reflector; such as its beam is able to be scanned to large angles with a phase shifter inserted into each element, and, for a space-deployable antenna, the piecewise flat surfaces in some cases are easier to fold into a smaller stowed volume. In order to mitigate the bandwidth problem, a recent technique of using multi-layer stacked-patch element [38] not only has increased the element bandwidth but also has reduced the effect of differential spatial phase delay. As a net result, the bandwidth has increased from a few percent to more than ten percent. Multi-band techniques can also be applied to

the reflectarray. Recently, two dual-band techniques have been developed for the X- and Ka-band frequencies. One used double-layer with two different-size rings and variable angular rotations [43], and the other also used double-layer with X-band crossed dipoles over Ka-band patches [44]. To summarize, although the narrow bandwidth characteristic is the primary shortcoming of a reflectarray, several techniques can be employed to improve the bandwidth performance.

10.5 Applications and Recent Developments

In addition to those possible reflectarray applications mentioned in the introduction and review sections, there are several other important applications and recent developments. One is a Ka-band circularly polarized inflatable reflectarray [39] with a 3-m-diameter aperture developed by the JPL for NASA's future spacecraft communication antenna application. As shown in Fig. 10-5, the antenna uses a torus-shaped inflatable tube to support and tension a 3-m thin-membrane reflectarray surface. This circularly polarized reflectarray, having approximately 200 thousand elements using variable angular rotation technique [8,39], is considered electrically the largest reflectarray ever build. Because the reflectarray has a "natural" flat surface, it is much easier for the inflatable structure to maintain its required surface tolerance (0.2 mm rms in this case) than a "non-natural" parabolic surface; in particular, for long-duration space flight. This inflatable antenna was later improved to equip with rigidizable inflatable tubes [39,49] in order to survive the hazardous space environment, such as bombardment by space debris and strenuous thermal effects. This reflectarray achieved an aperture efficiency of 30 percent with room for improvement and excellent far-field pattern shape with average sidelobe and cross-polarization levels below–40 dB, as shown in Fig. 10-7.

A second important development of the reflectarray is the achievement of a shaped contour beam by using a phase-synthesis technique. This reflectarray, shown in Fig. 10-37, was developed by the University of Massachusetts [37] for a commercial application to provide Earth contour-beam coverage. A typical calculated contour beam transmitted by this antenna, using a phase synthesis technique, is given in Fig. 10-38. Since a reflectarray generally has many thousands of elements, it thus has many degrees of freedom in design to provide an accurate and uniquely required contour beam.

A third important development is a dual-frequency reflectarray, where the two frequencies are widely separated, such as the X-band and Ka-band. The prototype antenna developed, shown in Fig. 10-39, is circularly polarized and uses variable-angularly-rotated annular rings [43]. It was developed by the Texas A&M University for JPL/NASA's future space communication application. This antenna, with a diameter of 0.5 m, uses a multi-layer technique in which the X-band annular rings are placed above the Ka-band

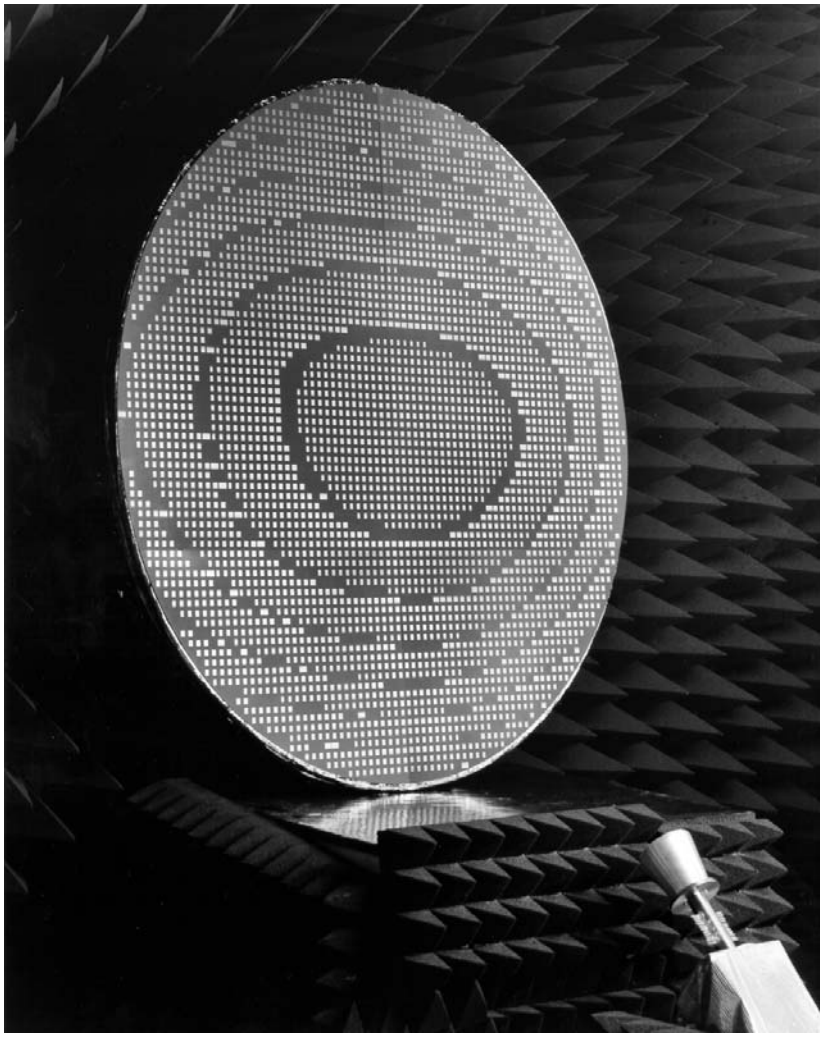

Fig. 10-37. Ku-band reflectarray with shaped contour beam capability [37]. (Courtesy of Professor Dave Pozar, Univ. of Massachusetts)

rings and serve as a frequency-selective surface to let the Ka-band signal pass through. The measured results indicate that the presence of the Ka-band elements has very little impact on the X-band performance. The measured radiation patterns of the Ka-band reflectarray without and with the X-band layer are shown in Figs. 10-40 and 10-41, respectively. There is no significant difference between the two patterns. However, the measured Ka-band gain of the dual-frequency dual-layer antenna is about 1.0 dB lower than the Ka-band alone antenna. The Ka-band alone reflectarray has a measured aperture

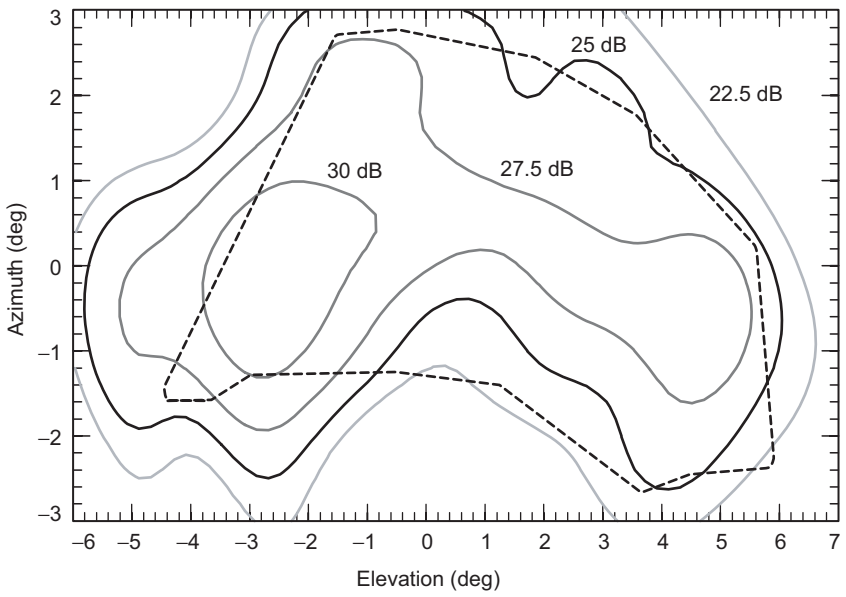

Fig. 10-38. A measured contour beam plot of the reflectarray shown in Fig. 10-26.

efficiency of 50 percent, while the dual-frequency dual-layer antenna has a Ka-band efficiency of about 40 percent. In other words, the X-band annular rings did impact the Ka-band performance somewhat. Future development work is needed to minimize this impact.

One final recent development is a reflectarray having a rectangular aperture intended for the NASA/JPL Wide Swath Ocean Altimeter (WSOA) radar application. This reflectarray uses variable-size patches as elements. The required rectangular aperture, as shown in Fig. 10-42, consists of five flat sub-apertures that are connected together to form a curved reflectarray [50]. The curving of the long dimension of the rectangular surface is to minimize the incident angles from the feed for the end elements, and thus, to optimize the radiation efficiency for all elements. The radiation efficiency here indicates the measured amount of energy of each element that is reradiated in the desired main beam direction. The advantage of using a reflectarray with flat subapertures is that it allows mechanically folding of the flat panels into a compact structure for spacecraft launch-vehicle stowage. Preliminary test data indicate that this reflectarray is functioning properly and some minor improvements are currently being carried out.

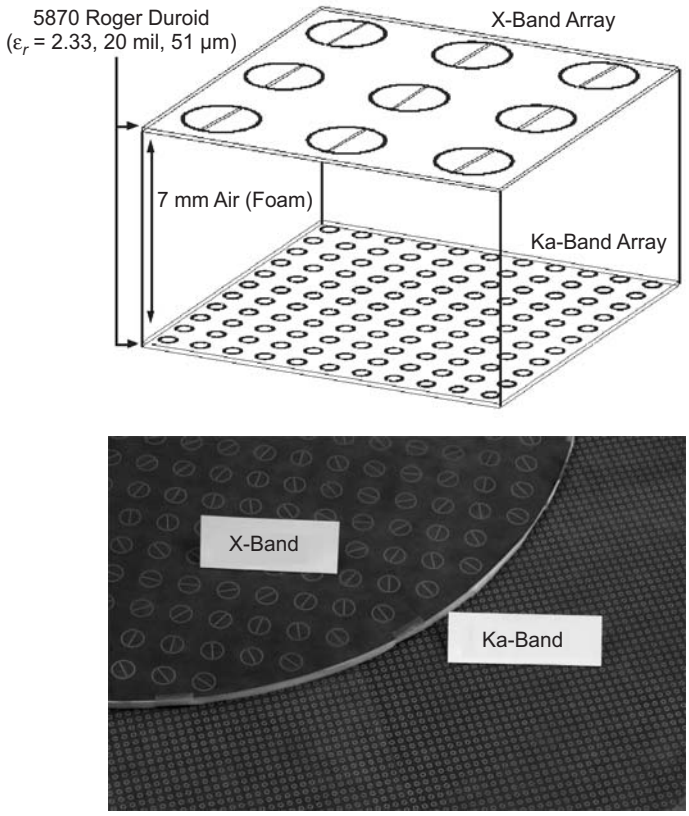

Fig. 10-39. The sketch and photo of the X/Ka dual-band two-layer reflectarray antenna using annular ring elements.

10.6 Summary

The reflectarray antenna has come a long way. However, its development and application had not been widely adapted until about the mid 1990s when the printable microstrip reflectarray was introduced. Except for its narrow bandwidth characteristic, the reflectarray has many advantages over a parabolic reflector antenna type. The main beam of a reflectarray can be designed to tilt to a large angle from its broadside direction. Phase shifters can be implanted into the elements for wide-angle electronic beam scanning. For large-aperture spacecraft antenna applications, the reflectarray's flat surface allows the antenna to be made into an inflatable structure, and it is easier to maintaining its surface tolerance than a curved parabolic surface. Its flat surface also can be made of multiple flat panels for ease in folding into a more compact structure

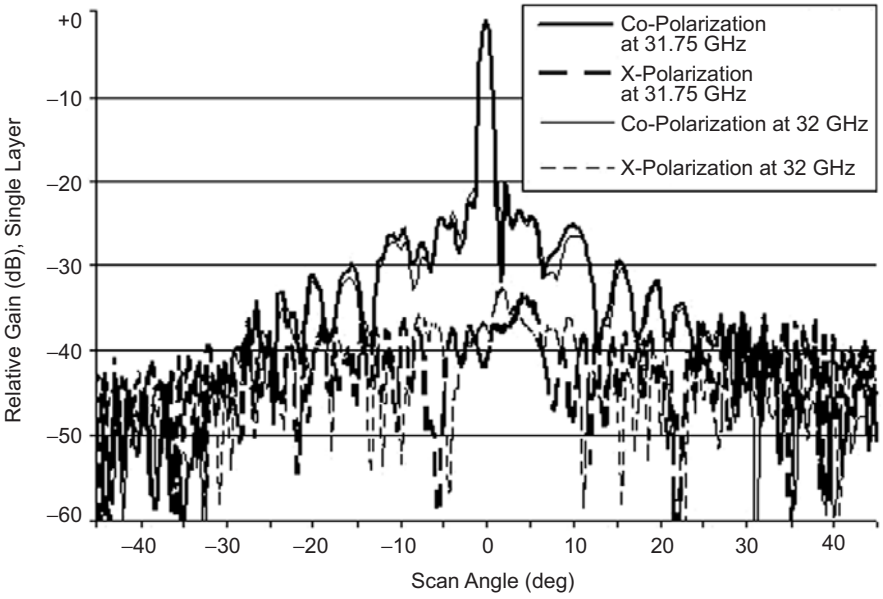

Fig. 10-40. Measured radiation pattern of the single-layer Ka-band reflectarray without the top X-band layer.

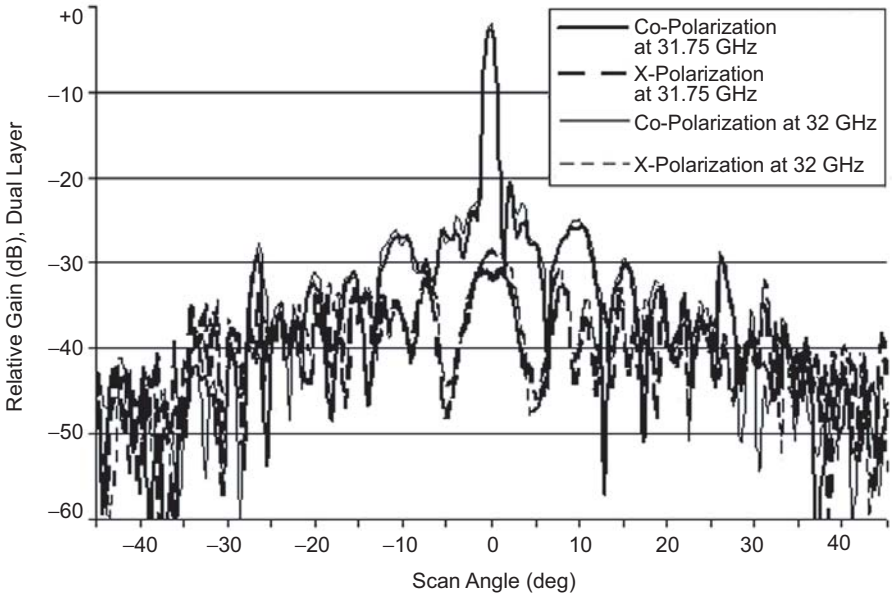

Fig. 10-41. Measured Ka-band radiation pattern of the two-layer X-/Ka-dual-band reflectarray.

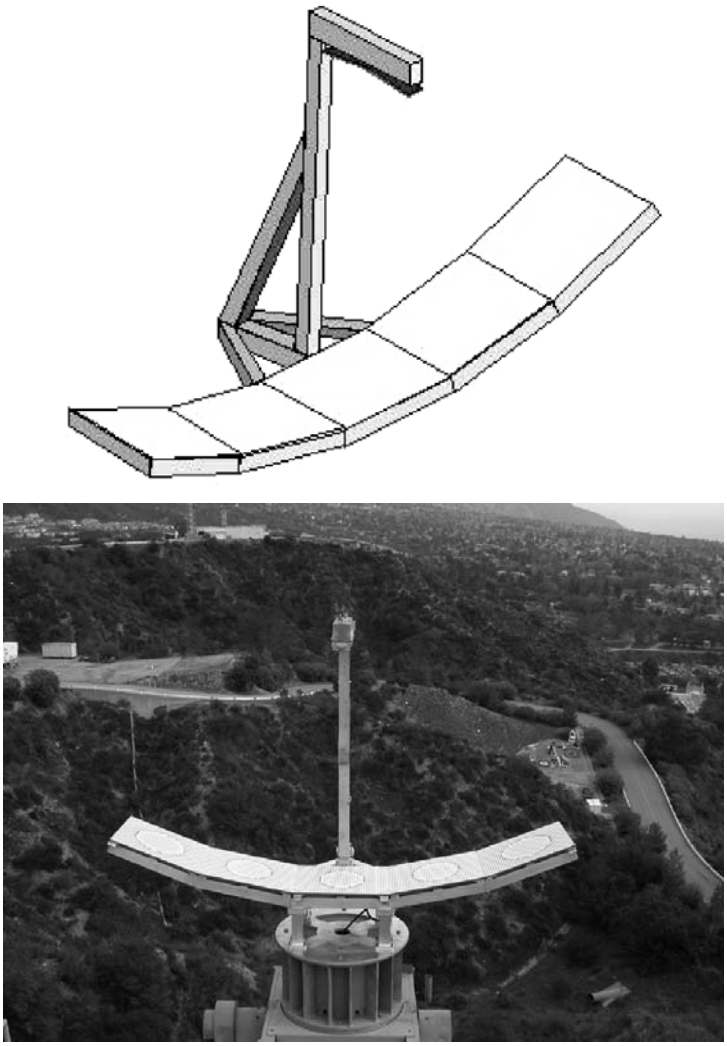

Fig. 10-42. Drawing and photo of the piece-wise flat reflectarray for space application.

for launch vehicle stowage. Very accurate beam shape can be achieved with phase synthesis for Earth-contour beam-coverage applications. Due to these many capabilities, the door has just opened for the development, research, and application of printed reflectarray antennas. Two major areas that need continuing improvement of the reflectarray performance are its bandwidth and its radiation efficiency.

References

[1] R. A. Russell, T. G. Campbell and R. E. Freeland, "A Technology Development Program for Large Space Antennas," *International Astronautical Congress*, 31st (Tokyo, Japan), IAF Paper 80-A-33, International Astronautical Federation, Paris, France, September 1980.

[2] G. Veal and M. Thomas, *Highly Accurate Inflatable Reflectors, Final Report*, AFRPL Report TR84-021, Air Force Rocket Propulsion Laboratory (renamed Air Force Astronautics Laboratory in 1987), Edwards Air Force Base, California, May 1984.

[3] R. E. Freeland, G. D. Bilyeu, and G. R. Veal, "Large Inflatable Deployable Antenna Flight Experiment Results," IAF paper 97-1.3.01, *48th Congress of the International Astronautical Federation* (Turin, Italy), International Astronautical Federation, Paris, France, October 1997.

[4] J. Huang, M. Lou, and E. Caro, "Super-Low-Mass Spaceborne SAR Array Concepts," 1997 *IEEE Antennas and Propagation Society International Symposium Digest*, 1997, vol. 2, pp. 1288–1291, July 13–18, 1997.

[5] J. Huang, "Emerging Array Antenna Technologies at JPL," *Antenna Technology and Applied Electromagnetics (ANTEM) Symposium* (Ottawa, Canada), August 1998.

[6] J. Huang, "The Development of Inflatable Array Antennas," *IEEE Antennas and Propagation Magazine*, vol. 43, pp. 44–50, August 2001.

[7] D. M. Pozar, "Microstrip Antenna Aperture-Coupled to a Microstripline," *Electronics Letters*, vol. 21, pp. 49–50, January 1985.

[8] J. Huang and R. J. Pogorzelski, "A Ka-Band Microstrip Reflectarray with Elements Having Variable Rotation Angles," *IEEE Transactions on Antennas and Propagation*, vol. 46, pp. 650–656, May 1998.

[9] H. Fang, M. Lou, J. Huang, L. Hsia, and G. Kerdanyan, "An Inflatable/Self-Rigidizable Structure for the Reflectarray Antenna," *10th European Electromagnetics Structure Conference* (Munich, Germany), EADS Deutschland GMbH, Munich, Germany, pp. 166–174, October 2001.

[10] H. Fang, M. Lou, J. Huang, U. Quijano, and L. Hsia, "Thermal Distortion Analysis of a Three-meter Inflatable Reflectarray Antenna," *44th AIAA/ASME/ASCE/AHS Structure and 4th AIAA Gossamer Spacecraft Forum* (Norfolk, Virginia), Paper 2003-1650, American Institute of Aeronautics and Astronautics, Reston, Virginia, April 2003.

[11] S. Schwartz, "Space Rigidization Techniques for Expandable Structures," *Modern Plastics*, vol. 46, p. 11, November 1969.

[12] W. F. Hinson and L. S. Keafer, Large Inflated Antenna Systems, NASA Report N84-17234, National Aeronautics and Space Administration, Washington, District of Columbia, 1984.

[13] L. B. Keller, S. Schwartz, A. Olivitch, and S. Allinikov, "Space Rigidizable Resin Fiberglass Sandwich Materials," *Journal of Spacecraft and Rockets*, vol. 3, pp. 513–518, April 1966.

[14] R. L. Jordan, "The Seasat-A Synthetic Aperture Radar System," *IEEE Journal of Ocean Engineering*, vol. OE-5, pp. 154–164, April 1980.

[15] E. R. Caro, "SIR-C, the Next Generation Spaceborne SAR," *The 2nd Spaceborne Imaging Radar Symposium*, Jet Propulsion Laboratory, Pasadena, California, pp. 203–217, 1987.

[16] J. Huang, M. Lou, B. C. Lopez, and E. Gama, "Foldable Frame-Supported Thin-Membrane Array," *Proceedings of 2000 International Symposium on Antennas and Propagation (ISAP 2000)* (Fukuoka, Japan), Communications Society of the Institute of Electronics, Information, and Communication Engineers (IEICE), Japan, pp. 213–216, August 2000.

[17] R. L. Jordan, B. L. Huneycutt, and M. Werner, "The SIR-C/X-SAR Synthetic Aperture Radar System," *IEEE Transactions on Geoscience and Remote Sensing*, vol. 33, pp. 829–839, July 1995.

[18] A. Moussessian, G. Sadowy, L. Del Castillo, J. Huang, S. Madsen, W. Edelstein, and A. Shapiro, "Transmit/Receive Membranes for Large Aperture Scanning Phased Arrays," *Earth Science Technology Conference (ESTC)* (College Park, Maryland), National Aeronautics and Space Administration Headquarters, Washington, District of Columbia, June 2003.

[19] J. Huang and A. Moussessian, "Thin-Membrane Aperture-Coupled L-Band Patch Antenna," *IEEE 2004 Antennas and Propagation Society Symposium Digest* (June 20–25, 2004, Monterey, California), vol. 3, IEEE, pp. 2388–2391, 2004.

[20] D. G. Berry, R. G. Malech, and W. A. Kennedy, "The Reflectarray Antenna," *IEEE Transactions on Antennas and Propagation*, vol. AP-11, pp. 645–651, November 1963.

[21] H. R. Phelan, "Spiraphase Reflectarray for Multitarget Radar," *Microwave Journal*, vol. 20, pp. 67–73, July 1977.

[22] R. E. Munson and H. Haddad, "Microstrip Reflectarray for Satellite Communication and RCS Enhancement and Reduction," United States patent 4,684,952, Washington, District of Columbia, August 1987.

[23] J. Huang, "Microstrip Reflectarray," *1991 IEEE Antennas and Propagation Symposium*, (London, Ontario, Canada), IEEE, pp. 612–615, June 1991.

[24] T. A. Metzler, *Design and Analysis of a Microstrip Reflectarray*, Ph. D. Dissertation, University of Massachusetts, Amherst, September 1992.

[25] Y. Zhang, K. L. Wu, C. Wu, and J. Litva, "Microstrip Reflectarray: Full-Wave Analysis and Design Scheme," *IEEE AP-S/URSI Symposium* (Ann Arbor, Michigan), pp. 1386–1389, June 1993.

[26] R. D. Javor, X. D. Wu, and K. Chang, "Beam Steering of a Microstrip Flat Reflectarray Antenna," *1994 IEEE International Antennas and Propagation Symposium* (AP-S/URSI, Seattle, Washington), pp. 956–959, June 1994.

[27] D. C. Chang and M. C. Huang, "Multiple Polarization Microstrip Reflectarray Antenna with High Efficiency and Low Cross-Polarization," *IEEE Transactions on Antennas and Propagation*, vol. 43, pp. 829–834, August 1995.

[28] A. Kelkar, "FLAPS: Conformal Phased Reflecting Surfaces," *Proceedings of the 1991 IEEE National Radar Conference* (Los Angeles, California), pp. 58–62, March 1991.

[29] D. M. Pozar and T. A. Metzler, "Analysis of a Reflectarray Antenna Using Microstrip Patches of Variable Size," *Electronics Letters*, pp. 657–658, April 1993.

[30] J. Huang, "Bandwidth Study of Microstrip Reflectarray and a Novel Phased Reflectarray Concept," *IEEE AP-S/URSI Symposium* (Newport Beach, California), pp. 582–585, June 1995.

[31] F. S. Johansson, "A New Planar Grating-Reflector Antenna," *IEEE Transactions on Antennas and Propagation*, vol. 38, pp. 1491–1495, September 1990.

[32] Y. T. Gao and S. K. Barton, "Phase Correcting Zonal Reflector Incorporating Rings," *IEEE Transactions on Antennas and Propagation*, vol. 43, pp. 350–355, April 1995.

[33] J. M. Colin, "Phased Array Radars in France: Present and Future," *IEEE Symposium on Phased Array Systems and Technology* (Boston, Massachusetts), pp. 458–462, October 1996.

[34] A. A. Tolkachev, V. V. Denisenko, A. V. Shishlov, and A. G. Shubov, "High-Gain Antenna System for Millimeter-Wave Radars with Combined Electrical and Mechanical Beam Steering," *IEEE Symposium on Phased Array Systems and Technology* (Boston, Massachusetts), pp. 266–271, October 1996.

[35] J. Huang and A. Feria, "A 1-m X-Band Inflatable Reflectarray Antenna," *Microwave and Optical Technology Letters*, vol. 20, pp.97–99, January 1999.

[36] J. Huang, "Capabilities of Printed Reflectarray Antennas," *IEEE Symposium on Phased Array Systems and Technology* (Boston, Massachusetts), pp. 131–134, October, 1996.

[37] D. M. Pozar, S. D. Targonski, and R. Pokuls, "A Shaped-Beam Microstrip Patch Reflectarray," *IEEE Transactions on Antennas and Propagation*, vol. 47, pp. 1167–1173, July 1999.

[38] J. A. Encinar, "Design of Two-Layer Printed Reflectarray Using Patches of Variable Size," IEEE Transactions on Antennas and Propagation, vol. 49, pp. 1403–1410, October 2001.

[39] J. Huang, V. A. Feria, and H. Fang, "Improvement of the Three-Meter Ka-Band Inflatable Reflectarray Antenna," *IEEE AP-S/URSI Symposium* (Boston, Massachusetts), pp. 122–125, July 2001.

[40] M. Bialkowski, A. W. Robinson, and H. J. Song, "Design, Development, and Testing of X-Band Amplifying Reflectarrays," *IEEE Transactions on Antennas and Propagation*, vol. 50, pp. 1065–1076, August 2002.

[41] R. E. Zich, M. Mussetta, M. Tovaglieri, P. Pirinoli, and M. Orefice, "Genetic Optimization of Microstrip Reflectarrays," *IEEE AP-S/URSI Symposium* (San Antonio, Texas), pp. III-128–III-131, June 2002.

[42] B. Khayatian and Y. Rahmat-Samii, "Characterizing Reflectarray Antenna Radiation Performance," *IEEE AP-S/URSI Symposium* (Columbus, Ohio), vol. 3, pp. 298–301, June 2003.

[43] C. Han, B. Strassner, K. Chang, and J. Huang, "A Dual-Frequency 7/32 GHz Reflectarray Antenna," *Progress in Electromagnetics Research Symposium (PIERS)* (Honolulu, Hawaii), p. 526, October 2003.

[44] M. Zawadzki and J. Huang, "A Dual-Band Reflectarray for X- and Ka-Bands," *Progress in Electromagnetics Research Symposium (PIERS)* (Honolulu, Hawaii), p. 525, October 2003.

[45] W. Menzel, D. Pilz, and M. Al-Tikriti, "Millimeter-Wave Folded Reflector Antennas with High Gain, Low-Loss, and Low Profile," *IEEE Antennas and Propagation Magazine*, vol. 44, no. 3, pp. 24–29, June 2002.

[46] D. Pozar, S. D. Targonski, and H. D. Syrigos, "Design of Millimeter Wave Microstrip Reflectarrays," *IEEE Transactions on Antennas and Propagation*, vol. 45, pp. 287–296, February 1997.

[47] E. Girard, R. Moulinet, R. Gillard, and H. Legay, "An FDTD Optimization of a Circularly Polarized Reflectarray Unit Cell," *IEEE AP-S/URSI Symposium* (San Antonio, Texas), pp. III-136–III-139, June 2002.

[48] J. Huang, "Analysis of a Microstrip Reflectarray Antenna for Microspacecraft Applications," *The Telecommunications and Data Acquisition Progress Report 42-120, October–December 1994*, Jet Propulsion Laboratory, Pasadena, California, pp. 153–173, February 15, 1995. http://ipnpr.jpl.nasa.gov/progress_report/

[49] H. Fang, M. Lou, J. Huang, L. M. Hsia, and G. Kerdanyan, "An Inflatable/Self-Rigidizable Structure for the Reflectarray Antenna," *10th European Electromagnetic Structure Conference* (Munich, Germany), October, 2001.

[50] R. Hodges and M. Zawadzki, "Design of a Large Dual Polarized Ku-Band Reflectarray for Spaceborne Radar Altimeter," *IEEE AP-S Symposium* (Monterey, California), pp. 4356–4359, June 2005.